The binding mechanism of *Streptococcus suis* accessory virulence factor and adhesin SadP to globotetraosylceramide

Miralda Madar Johansson[1¶], Eva Bélurier[2¶#], Anastassios C. Papageorgiou[3], Anders P. Sundin[4], Jani Rahkila[5], Teemu Kallonen[6,9], Ulf J. Nilsson[4], Santeri Maatsola[2], Thomas K.M. Nyholm[7], Jarmo Käpylä[8], Jukka Corander[9], Reko Leino[10], Jukka Finne[11], Susann Teneberg[1], Sauli Haataja[2*]

[1]Department of Medical Biochemistry and Cell Biology, Institute of Biomedicine, Sahlgrenska Academy at University of Gothenburg, Gothenburg, Sweden

[2]Institute of Biomedicine, Research Center for Cancer, Infections and Immunity, University of Turku, Turku, Finland

[3]Turku Bioscience Centre, University of Turku and Åbo Akademi University, Tykistökatu 6, FI-20520 Turku, Finland

[4]Centre for Analysis and Synthesis, Department of Chemistry, Lund University, POB 124, SE-221 00 Lund, Sweden

[5]Instrument Centre, Åbo Akademi University, FI-20500 Turku, Finland

[6]Department of Biostatistics, University of Oslo, Blindern, 0317, Norway and Department of Clinical Microbiology, Turku University Hospital, Turku, Finland

[7]Biochemistry Faculty of Science and Engineering, Åbo Akademi University, FI-20500 Turku, Finland.

[8]Department of Biochemistry, University of Turku, FI-20014 Turku, Finland

[9]Parasites and Microbes, Wellcome Sanger Institute, Cambridge, United Kingdom, Department of Biostatistics, University of Oslo, Blindern, 0317, Norway and Helsinki Institute for Information Technology HIIT, Department of Mathematics and Statistics, University of Helsinki, 00014 Finland

[10]Laboratory of Molecular Science and Technology, Åbo Akademi University, FI-20500 Turku, Finland

[11]Molecular and Integrative Biosciences Research Programme, Faculty of Biological and Environmental Sciences, University of Helsinki, P.O. Box 56, FI-00014, Helsinki, Finland

[#]Current address: Faculté des Sciences et Technologies (Sciences and Technology Faculty), University of Lille, Lille, France

[*]Corresponding author

E-mail: sauli.haataja@utu.fi

[¶]equal contribution

Abstract

Streptococcus suis is part of the pig commensal microbiome and a major pig pathogen causing pneumonia and meningitis, occasionally also in humans. The genomic analysis divides *S. suis* to asymptomatic carriage, respiratory and invasive systemic strains with distinct genomic signatures. The virulence factor *S. suis* adhesin P (SadP) recognizes the galabiose Galα1–4Gal-oligosaccharide. Based on the oligosaccharide fine specificity, SadP can be divided into subtypes P_N and P_O. We show that subtype P_N is distributed in the systemic strains. Both types of SadP are shown to predominantly bind to pig lung globotriaosylceramide (Gb3). SadP adhesin from virulent subtype P_N strain also binds to globotetraosylceramide (Gb4). Mutants of type P_N SadP adhesin were constructed into the galabiose-binding domain and analyzed to reveal the mechanism for Gb4 binding. Functional and structural analysis of type P_N SadP mutants showed that amino acid N285 of the galabiose-binding site was required for binding to Gb4 and strikingly was also required for interaction with the glycomimetic inhibitor phenylurea-galabiose. Molecular dynamics simulations provided further insight into the role of N285 for Gb4 and phenylurea-galabiose binding, suggesting additional hydrogen bonding to terminal GalNAc of Gb4 and urea-group. Importantly, type P_N SadP adhesin expressed by strains causing invasive systemic disease binds via a distinct amino acid N285 mediated mechanism to Gb4. Thus, this molecular mechanism of type P_N SadP binding is a candidate for selectively targeting *S. suis* meningitis without interfering with commensal strains, which opens up new venues for developing intervention strategies against this pathogen.

Author summary

Streptococcus suis is a major pig pathogen, which occasionally also causes meningitis in humans. Despite the wealth of existing genomic data, the mucosal surface colonizing mechanisms of these streptococci are poorly understood. *S. suis* population evolves rapidly and is prone to acquire antibiotic resistance factors and could hamper the efficacy of vaccines by serotype replacement. The accessory genomes of specific subpopulations are expected to encode factors that are associated with particular ecological niches and

enhanced pathogenicity. By identification of such accessory factors we could aim to develop clinical interventions targeting the pathovariants while leaving commensal bacteria unharmed, which would mitigate harmful serotype replacement. In this study we identified by both genomic and structure-function analysis the accessory *S. suis* virulence factor SadP as specific for population causing meningitis. The presented data provide an insight into a molecular mechanism how a single amino acid change can cause a functional divergence in host cell glycolipid receptor binding in emerged meningitis pathovariant of streptococci. The results can be utilized to design population- and ecology aware means to target infectious disease caused by this pathogen.

Introduction

Bacterial adhesion to host cell surfaces is a prerequisite for infectious disease. Host cell surfaces are heavily covered by surface carbohydrates that form the glycocalyx layer [1,2]. Pathogenic bacteria and their toxins can treacherously exploit carbohydrates to attach and invade cells. One example is a group of endogenous glycosphingolipids, known as globo series membrane glycosphingolipids, which are grouped based on the Galα1–4Gal (galabiose) structure. Globo series glycolipids are cellular receptors for toxic action of Verotoxins and for the attachment of bacteria, such as uropathogenic *Escherichia coli*, *Streptococcus suis* and *Pseudomonas aeruginosa* [3–6].

Since antibiotics are increasingly losing their power, alternative antimicrobial compounds need to be invented and developed [7,8]. Transformation of bacteria to antibiotic-resistant forms can be overcome by developing compounds that block *in vivo* colonization and virulence factors without killing the pathogens. Cell surface carbohydrate glycomimetics are the most tempting pipeline for the development of new generation of antimicrobials [9,10].

Streptococcus suis is an important pig pathogen causing septicemia, pneumonia and meningitis. It also causes severe zoonotic meningitis. Recent data show that it is a major pathogen of pigs and produces an alarmingly vast array of factors causing high antibiotic resistance [11]. The pathogenic types of *S. suis* are efficiently transmitted from host to host and the bacterium can be frequently isolated from the tonsils as a carrier strain. However, unfortunately predisposed by environmental factors such as overcrowding and

synergistic activities with other keystone pathogens [12], *S. suis* invades the host tissues and by expressing both soluble and cell wall bound virulence factors aggravates tissue damage in the critical organs and causes death [13,14].

S. suis strains expressing SadP adhesin bind specifically to Galα1–4Gal-containing oligosaccharides [15]. Interestingly, galabiose-binding strains can be divided to subtypes P_N and P_O based on how they recognize galabiose-containing carbohydrates in hemagglutination assays [16]. Type P_N strains recognize galactose, *N*-Acetylgalactosamine, and the ceramide-linked oligosaccharides Gb3 (Galα1–4Galβ1–4Glc) and Gb4 (GalNAcβ1–3Galα1–4Galβ1–4Glc). Subtype P_O recognizes only galactose and preferentially binds to Gb3. Recently, *S. suis* galabiose-binding adhesin SadP was identified as an LPNTG-anchored cell-wall protein [6]. The carbohydrate interaction of SadP has been shown to mediate *S. suis* binding to pharyngeal epithelium and intestinal epithelial cells [16,17]. In an *S. suis* murine infection model, the mice deficient in globotriaosyl ceramide (Gb3) expression (knockout in alpha-1,4-galactosyltransferase A4GALT) developed less severe brain inflammation and injury [18]. Recently, low picomolar concentrations of glycomimetic 3-phenylurea-galabiose-containing dendrimers were shown to block *S. suis* SadP (type P_N) adhesin binding activity [19]. However, the molecular basis of differences in galabiose-binding mechanisms of SadP adhesins have remained elusive. In the present study, we have characterized the pig Galα1–4Gal-containing receptors in porcine lung tissue using mass spectrometry and thin layer chromatography (TLC) overlay assay. The binding mechanism of type P_N, P_O and site-specific mutants of type P_N SadP to globosyl oligosaccharides were studied. The results show that *S. suis* SadP specifically recognizes globo series glycolipids isolated from the pig lungs and that specific amino acid changes in the proximity of the galabiose-binding site have an effect on the SadP type P_N and P_O specificity.

Results

Sequence analysis of SadP subtypes P_N and P_O, structural modelling and distribution in *S. suis* systemic, respiratory and non-clinical strains

SadP adhesins are 80 kDa LPNTG-anchored cell-wall proteins, which contain the signal sequence for secretion, the N-terminal galabiose binding domain, tandem repeat domains and C-terminal LPNTG cell-wall

anchor domain [6]. The galabiose-binding domains have no significant sequence homologs to other bacterial proteins or to other carbohydrate binding domains. The SadP N-terminal galabiose-binding domains (aa125-328) of hemagglutinating type P_N and type P_O strains were cloned, sequenced and compared with multiple alignment (Fig 1A). The structure consists of three α-helixes and ten β-strands (β1-β10) that form a β-sandwich core domain. The sequences of the N-terminal galabiose-binding domain of type P_N SadP adhesins are 100 % identical and are found in virulent serotype 2 strains. There is more sequence variation in the galabiose-binding site of type P_O SadP. The carbohydrate binding sites of types P_N and P_O are highly conserved (Fig 1B). Interestingly there is a conservative change at position 285 from asparagine to aspartate, which could have an effect for the interaction of type P_N SadP with GalNAcβ1–3Galα1–4Gal-oligosaccharide.

The distribution of *sadP* genes in clinical and non-clinical strains analyzed with core genome phylogeny analysis is shown in Figure 1C. The gene of *sadP* type P_N was found in 91.9 % of systemic *S. suis* isolates (88.1 % of strains isolated from brain), whereas only less than 1 % of strains had the gene encoding *sadP* type P_O. Based on the maximum-likelihood core genome phylogeny analysis the type P_N SadP gene is found in clonal virulent *S. suis* strains, which mostly belong to serotype 2. Interestingly, also serotype 14 strains isolated from human meningitis cases have type P_N gene. Type P_O *sadP* was found more frequently in respiratory and non-clinical strains.

Purification and analysis of glycosphingolipid composition of porcine lung

The interaction of recombinant SadP with globo series glycolipids has not been thoroughly characterized. Moreover, whether SadP binds to Gb3 or Gb4 isolated from the pig tissues has not yet been directly shown. The glycolipids were isolated from porcine lung and erythrocytes, in order to control that the glycolipids isolated from the lungs were not contaminants derived from the erythrocytes remaining in the lungs. The total non-acid glycosphingolipid fractions were hydrolyzed with endoglycoceramidase II of *Rhodococcus* sp., and the oligosaccharides thereby obtained were analyzed by LC-ESI/MS using graphitized carbon columns. This method gives resolution of isomeric oligosaccharides, and the MS^2 analyses gives complete sequence information and allows differentiation of linkage positions by diagnostic cross-ring ^{0,2}A-type fragment ions [20].

147 The base peak chromatograms from LC-ESI/MS of the oligosaccharides obtained by hydrolysis of the
148 total non-acid glycosphingolipid fractions of porcine erythrocytes and lung are shown in Figure 2A. By
149 comparison of the retention times and MS^2 spectra of oligosaccharides obtained from reference
150 glycosphingolipids, the major oligosaccharides obtained from porcine lung were tentatively identified as
151 globotriaosylceramide (Gb3, detected as a $[M-H^+]^-$ ion at *m/z* 503) and the blood group H type 2
152 pentasaccharide (H5-2, detected as a $[M-H^+]^-$ ion at *m/z* 852) (Figure 2A). The major oligosaccharides from
153 porcine erythrocytes were globotriaosylceramide (Gb3, detected as a $[M-H^+]^-$ ion at *m/z* 503),
154 globotetraosylceramide (Gb4, detected as a $[M-H^+]^-$ ion at *m/z* 706), and the blood group A type 2
155 hexasaccharide (A6-2, detected as a $[M-H^+]^-$ ion at *m/z* 1055) (Fig 2B). Thus, globotriaosylceramide was found
156 in both samples, but otherwise the two samples were significantly different. The total non-acid
157 glycosphingolipid fraction from porcine lung was thereafter separated by Iatrobeads chromatography. Aliquots
158 of the fractions obtained were analyzed by thin-layer chromatography, and fractions that were coloured green
159 by anisaldehyde were tested for binding of SadP using the chromatogram binding assay. The fractions were
160 thereafter pooled according to the mobility on thin-layer chromatograms and their SadP binding activity.
161

162 **The binding of SadP to neutral glycolipids isolated from porcine lung using TLC overlay**
163 **assay**

164 The separations gave two SadP binding fractions migrating in the triglycosylceramide region. One
165 fraction (0.2 mg) migrating as a single band was denoted fraction PL-1 (Fig 2B, lane 1), and one fraction (0.3
166 mg) migrating as a double band was denoted fraction PL-2 (Fig 2B, lane 2). In addition, one SadP binding
167 fraction (0.4 mg) with compounds migrating as tetraglycosylceramides was obtained (denoted fraction PL-4;
168 Fig 2B, lane 4).
169

170 **LC-ESI /MS of native SadP binding glycosphingolipids from porcine lung**

171 ESI/MS of the native fraction PL-1 gave a major $[M-H^+]^-$ ion at *m/z* 1132 (S1A Fig), indicating a
172 glycosphingolipid with three Hex, and sphingosine with non-hydroxy 24:1 fatty acid. MS^2 of the $[M-H^+]^-$ ion

at *m/z* 1132 gave a series of Y ions (Y_0 at *m/z* 646, Y_1 at *m/z* 808, and Y_2 at *m/z* 970) demonstrating a Hex-Hex-Hex sequence combined with sphingosine with non-hydroxy 24:1 fatty acid (S1B Fig).

A $[M-H^+]^-$ ion at *m/z* 1132 was also obtained by ESI/MS of the native fraction PL-2 (S2 Fig). Here, the major $[M-H^+]^-$ ion was seen at *m/z* 1022 (S2AB Fig), demonstrating a glycosphingolipid with three Hex, and sphingosine with non-hydroxy 16:0 fatty acid. Also, here a Hex-Hex-Hex sequence was demonstrated by the series of Y ions (Y_0 at *m/z* 536, Y_1 at *m/z* 698, and Y_2 at *m/z* 860) from MS^2 (S2D Fig).

Endoglycoceramidase digestion and LC-ESI /MS of SadP binding glycosphingolipids from porcine lung

The base peak chromatograms from LC-ESI/MS of the oligosaccharides obtained by endoglycoceramidase digestion of fractions PL-1 and PL-2 were very similar (S3AB Fig). Both had a $[M-H^+]^-$ ion at *m/z* 503 which eluted at the same retention time (17.4-18.4 min) as the saccharide obtained from reference globotriaosylceramide (S3C Fig), while the saccharide from reference isoglobotriaosylceramide eluted at 20.0-20.4 min (Figure S3D).

MS^2 of the ion at *m/z* 503 of fractions PL-1 and PL-2 gave in both cases two C-type fragment ions (C_1 at *m/z* 179 and C_2 at *m/z* 341) identifying a Hex-Hex-Hex sequence (Figure S3EF). A 4-substitution of the internal Hex was demonstrated by the $^{0,2}A_2$ fragment ion at *m/z* 281 [20–22] . Taken together with the similarity to the MS^2 spectrum of reference globotriaosyl saccharide (S3G Fig), this allowed identification of the saccharides of fractions PL-1 and PL-2 as globotriaosyl saccharides (Galα1–4Galβ4Glc).

LC-ESI/MS of the oligosaccharides obtained by hydrolysis of fraction PL-4 with *Rhodococcus* endoglycoceramidase II allowed a tentative identification of a globotetraosyl saccharide (GalNAcβ1–3Galα1–4Galβ1–4Glc). This conclusion was based on the following spectral features: First, the base peak chromatogram of fraction PL-4 had a $[M-H^+]^-$ ion at *m/z* 706 (Figure S4A), and MS^2 of this ion (S4B Fig) gave a C-type fragment ion series (C_1 at *m/z* 220, C_2 at *m/z* 382, and C_3 at *m/z* 544), demonstrating a HexNAc-Hex-Hex-Hex sequence. The $^{0,2}A_3$ fragment ion at *m/z* 484 demonstrated a 4-substituted Hex, while the $^{0,2}A_4$ ion at *m/z* 646, and the $^{0,2}A_4$-H_2O ion at *m/z* 628, were derived from cross-ring cleavage of the 4-substituted Glc of

199 the lactose unit at the reducing end. The features of this MS^2 spectrum were very similar to the MS^2 spectrum
200 of the reference globotetraosyl saccharide (S4C Fig)

201 The base peak chromatogram of fraction PL-4 (S4A Fig) also had two $[M-H^+]^-$ ions at *m/z* 998, eluting
202 at 19.4 min and 21.4 min. In both cases MS^2 demonstrated a Fuc.Hex-(Fuc-)HexNAc-Hex-Hex sequence, and
203 the diagnostic ion at *m/z* 348 (S4D Fig) identified a Le^b hexasaccharide, whereas the diagnostic ion at *m/z* 510
204 (S4E Fig) identified a Le^y hexasaccharide [21].

205

206 **SadP subtype P_N and P_O binding to purified glycolipids**

207 TLC overlay assay is a powerful method to analyze glycolipid receptor function. The carbohydrate-
208 binding specificity of SadP to globo series isoreceptors was determined using purified glycolipids (all TLC
209 binding results are summarized in Table 1). Type P_N bound preferentially to Gb3 and P1 glycolipid, and also
210 weakly to Gb4 and the Forssman glycolipid (Fig 2C). SadP type P_O also bound strongly to Gb3 and P1, i.e. to
211 glycolipids with terminal Galα1–4Gal, whereas there was no binding to Gb4 and the Forssman glycolipid (Fig
212 2D). There was no binding to the non-acid glycolipid fraction from the pig intestine, containing the Globo H.

213 The type P_N SadP binding to dilutions of globo series glycolipids was analyzed with TLC overlay assay
214 to the detection limit for the various glycolipids (S5A Fig). The full length adhesin bound mainly to P1
215 glycolipid, with a detection limit at 0.4 μg, whereas the detection limit for the Gb3 glycolipid was 0.8 μg. The
216 detection limit of SadP(31-328) *N*-terminal domain was 0.2 μg for both Gb3 and P1.

217 Next, the SadP binding to 250 ng of glycolipids immobilized in plastic microtiter wells was
218 quantitatively evaluated by solid phase binding assay (S5B Fig). No binding to the Gb2 glycolipid,
219 galabiosylceramide was detected, whereas there was weak binding to Galα1–4Galβ1–O-*bis*-$(SO_2\text{-}C_{16}H_{33})_2$.
220 SadP was found to bind stronger to Gb3 with non-hydroxy ceramide than to Gb3 with hydroxy ceramide.
221 There was also binding to Gb4 and iGb3 isoglobotriaosylceramide. Binding to P1 pentaosylceramide was at
222 the same level as binding to Gb3 with non-hydroxy ceramide. The difference in the binding to iGb3 (Galα1–
223 3Gal- containing glycolipid) in the microtiter well assay compared to TLC overlay assay could be due to the
224 difference in the presentation of the binding epitope and the clustering of the glycolipid moieties.

225

Galα1–4Gal-dependent endothelial cell binding activity of *S. suis* SadP

S. suis type P_N WT strain D282 and the corresponding mutant strain D282Δ*sadP,* containing an insertion mutation into SadP gene, were compared for their binding activity to cultured cell line EA.hy926, which is a primary human umbilical vein cell line fused with a thioguanine-resistant clone of A549 (human lung adenocarcinoma cell line). In addition, binding of purified fluorescently labelled SadP was analysed for the binding to EA.hy926 cells. The cells were grown into glass coverslips for 48 h and the bacteria grown into early log phase were added to cells and were let to adhere for 1 h. After washing and staining with DiffQuick the bacteria were enumerated. The average adherence of wild-type bacteria was calculated to be 8.7 ± 0.5 bacteria/field, whereas the mean adhesion of 1.3 ± 0.5 of the insertion mutant Δ*sadP* was significantly less (unpaired t test > 0.0001) (Fig 3A). In addition, the binding of the WT strain was inhibited with 10 μg/ml pigeon ovomucoid, which contains *N*-linked glycans with terminal Galα1–4Gal [23]. The inhibitor reduced the adherence of *S. suis* bacteria to the cells to 0.7 ± 0.1 bacteria/field.

For flow cytometry assay, the cells were grown in wells, washed and tested for the binding of FITC labelled SadP. After washing, the cells were harvested with scraping and analyzed with flow cytometer. The flow cytometry results (dot blot and the histogram) are presented in Figure 3BCD. The median SadP binding with and without inhibitor (pigeon ovomucoid, 10 μg/ml) were 56.2 and 14.9 per 10 000 total events (median of untreated cells was 12.8).

Fine specificities toward Gb3 and Gb4 oligosaccharide structures

Next, the ability of the type P_N SadP-D282(31-328) and P_O SadP-6407(31-328) recombinant adhesin constructs to recognize galabiose glycoconjugates was analyzed using isothermal titration calorimetry (Fig 4AB). Both type P_N and P_O adhesins were titrated with oligosaccharides representing the terminal epitopes of Gb3 and Gb4, the TMSEt (2-trimethylsilylethyl) glycosides of Galα1–4Gal and GalNAcβ1–3Galα1–4Gal [24]. The dissociation constant values (K_D) of type P_N SadP-D282(31-328) and type P_O SadP-6407(31-328) interaction with Galα1–4Gal were 13.0 ± 1.5 μM (n=0.85, ΔH=-69.0±2.0 and -TΔS=41.1) and 3.5 ± 1.6 μM (n=0.85, ΔH=-40.0±2.7 and -TΔS=8.8) respectively. The K_D for interaction of P_N and P_O adhesins with

GalNAcβ1–3Galα1–4Gal compared to Galα1–4Gal were 2.6-fold higher with type P_N (K_D= 33.7±3.5 μM, n=1.14, ΔH=-40.1±2.0 and -TΔS=14.0) and 269-higher with type P_O (K_D= 940±680 μM, n=0.13, ΔH=-197±5500 and -TΔS=179).

Then, both adhesins were analyzed with AlphaScreen competitive inhibition assay (Fig 4C) for their interaction with Galα1–4Gal in comparison to a glycomimetic inhibitor 3'-phenylurea-derivative (3'-phenylurea-Galα1–4Gal β1–methoxyphenyl), which is a low nanomolar inhibitor of type P_N SadP [19,25]. The binding of His-tagged recombinant adhesins to biotinylated pigeon ovomucoid was inhibited with the above oligosaccharides. The IC_{50} values of type P_N adhesin for Galα1–4Galβ1–methoxyphenyl and 3'-phenylurea-Galα1–4Gal β1–methoxyphenyl were 1 μM and 0.030 μM, whereas with type P_O adhesin the corresponding values were 0.3 μM and 70 μM respectively. Also 4 other recombinant type P_O SadP N-terminal-domains were tested using 10 μM inhibitor concentrations (Fig 4D). For all type P_O adhesins the inhibition obtained with the C3'-phenylurea-derivative was weaker than the inhibition obtained with Galα1–4Gal.

Site-specific mutation changes the specificity of type P_N recombinant adhesin to type P_O

The binding mechanism of type P_N and P_O SadP was further studied by site-directed mutagenesis. Type P_N adhesin SadP-D282(125-329) was mutated and the mutants were analyzed for the binding to galabiose oligosaccharides with AlphaScreen competitive inhibition assay and ITC. Multiple alignment of SadP homologues allowed us to predict amino acids from the galabiose-binding region that differed between type P_N and P_O (Fig 1A). Based on that, the site-specific amino acid change N285D and E292Q, deletion Δ244-246 and N285D&Δ244-246 mutants were constructed into the type P_N SadP(125-328) cloned into the plasmid pET28a. In addition, the 28 amino acid long region H216-D246 of the type P_N was replaced by the corresponding region of type P_O.

The WT SadP and mutants were expressed and purified as described in the methods and analysed with SDS-PAGE (S6 Fig). The galabiose-binding strengths of the above mutant constructs, full length SadP, SadP *N*-terminal constructs SadP(31-328), SadP(125-328) and as a negative control site-specific mutant SadP(31-

328)W258A, were compared by AlphaScreen asssay (S7 Fig). The binding of full-length SadP to biotinylated pigeon ovomucoid was weaker compared to the *N*-terminal domain constructs, which could be due to a larger size of the full length SadP. The size of the protein could increase the distance of the acceptor and donor beads, and hence reduce the transmission of the singlet oxygen during the assay [19]. As a negative control for the assay, there was no binding of site-specific mutant W258A to pigeon ovomucoid. Of the mutants in the type P_N SadP(125-328) background, mutants N285D and E292Q bound well whereas the binding of mutants Δ244-246 and H216-D246delinsDELFNRFPNKVDSTNNGDGAPFRFFNKE was reduced. The binding of N285D&Δ244-246 mutant was abolished.

Next the specificities of mutants were analyzed with AlphaScreen assay using phenylurea-derivative and Galα1–4Gal (S7B - F Figs). All mutants were equally inhibited by the Galα1–4Gal oligosaccharide, but only with the site-specific mutant N285D the inhibitory power of Phenylurea-Galα1–4Gal was weaker compared to Galα1–4Gal, suggesting a specific switch from type P_N to P_O specificity.

Next, the Alphascreen inhibition assay was used to compare the effect of site-specific mutation in N285D to the specificity between Galα1–4Gal (terminal Gb3 structure) and GalNAcβ1–3Galα1–4Gal (terminal Gb4 structure) TMSEt glycosides. SadP(125-329) type P_N and site-specific mutant N285D were similarly inhibited with Galα1–4Gal, whereas N285D was not inhibited with even higher concentrations of GalNAcβ1–3Galα1–4Gal (Fig 5AB).

The K_D values of type P_N SadP(125-328) and site-specific mutant N285D for oligosaccharides was analyzed with isothermal titration calorimetry (Fig 5C). The wild type SadP(125-329) K_D values for Galα1–4Gal and GalNAcβ1–3Galα1–4Gal were 3.4±0.09 (n=0.76, ΔH=92.0±0.3 and -TΔS=60.8) and 36.0±4.8 μM (n=0.56, ΔH=70.2±5.0 and -TΔS=44.7) respectively. The K_D of site specific mutant N285D with Galα1–4Gal was 22.7±7.2 μM (n=0.52, ΔH=26.8±5.4 and -TΔS=20.5) (6-fold increase compared to wild-type SadP), whereas there was no interaction between N285D and GalNAcβ1–3Galα1–4Gal. Thus, the above results suggest that N285 has a specific role in SadP type P_N binding to GalNAcβ1–3Galα1–4Gal.

The effect of N285D mutation to SadP binding to glycolipids incorporated into POPC and POPC-cholesterol liposomes was analyzed by dotting liposomes to PVDF membrane and binding of his-tagged adhesins to immobilized liposomes (Fig 6). WT SadP type P_N bound to Gb4 of both non-cholesterol and

cholesterol-containing liposomes, whereas there was no binding by N285D mutant. The acyl chain length or hydroxylation of ceramide had no major effects for Gb3 binding.

Structural comparison of recombinant SadP type P_N and its N285D mutant

The site-specific mutant SadP(125-329)N285D was crystallized with five molecules in the crystallographic asymmetric unit (Fig 7A, Table S1). All molecules are similar with subtle differences as suggested by the low root mean square deviation (r.m.s.d) between them (0.25-0.31 Å). The structure of the N285D mutant is similar to that of the native SadP (PDB id 5BOB) with r.m.s.d. of 0.26 Å for 199 aligned residues. The structure consists of three α-helixes and ten β-strands (β1-β10) that form a β-sandwich core domain (Fig 7B). The first β-sheet of the β-sandwich is formed by antiparallel β1-β10-β9-β4-β7-β6 strands and the second β-sheet by β2-β3-β8-β5 in antiparallel fashion.

Structural superposition with the Galα1–4Gal – Fhc structure revealed small differences (Fig 7C). The side chain of D285 was found slightly rotated compared to the N285 side chain in the wild type.

Resolution of the interaction mechanisms of SadP to globo series glycolipids and C3'-Phenylurea–Galα1–4Gal

The key amino acids of both types P_N and P_O are conserved. Y198, Q255, R238 and G233 forms hydrogen bonds with the HO–3', HO-4' and HO-6' of the α'-Gal and the K316 with HO-2 and HO-3 of the β-Gal pyranose ring. W258 most likely forms CH-π interactions with the hydrophobic face of the disaccharide (Fig 7C). Type P_N SadP N285 is on the edge of the binding pocket, and it potentially interacts with the terminal GalNAcβ1–3 of Gb4 or 3-phenylurea-group. To study the SadP interaction with the receptor saccharide Galα1–4Galβ1–4Glc in solution, STD-NMR was applied using type P_N SadP(125-329) and the corresponding mutant N285D (Fig 7D). STD-NMR results suggest that both the type P_N SadP and the mutant N285D interact mainly with the two terminal galactose units of Gb3. With the mutant N285D the interactions of H-4′ and H-4″ are, however, somewhat weaker compared to the interaction of H-6″. Additionally, the mutant N285D does

not seem to have a clear interaction with the β-glucoside unit at the reducing end of Gb3, whereas the type P_N SadP appears to have interactions with H-2, H-3 and H-4.

In order to find a plausible hypothesis explaining the binding preferences of the galabiose, GalNAcβ1–3Galα1–4Gal and phenylurea-galabioside for WT and the N285D mutant, molecular dynamic simulations of their respective complexes were performed. Briefly, the ligand structures were built without the TMSEt aglycon to simplify the simulations and were then placed in the binding site of SadP (pdb id 5BOA) with the Galα1–4Gal disaccharide oriented as in the crystal structure. The terminal GalNAcβ1 residue was oriented with the dihedral glycosidic bond angles minimized with the H1 parallel to H4' of Galα1–4Gal. The three complexes with WT were mutated by exchanging N285 for D285. The complexes were unrestrainedly subjected to 100 ns molecular dynamics simulations and all starting conformations converged towards similar stable complex geometries (Fig 8A-E), except for the phenylurea derivative in complex with the N285D mutant for which light constraints on the backbone atoms of protein secondary structures were applied (Fig 8F). The α-face of the β-galactoside residue of all three ligands stacked to W258 forming CH-π interactions and the galabiose disaccharide moiety in all simulations retained the interactions and hydrogen bonds observed in the X-ray structure with the Gb3 trisaccharide (PDB id 5boa). The HO-4' of galabiose did not interact directly with N285, but instead via N285 sidechain NH hydrogen bond donation to a network of hydrogen bonds involving 3-5 water molecules and the G233 carbonyl oxygen (Fig 8A and S9 movie). Mutation of N285 to D285 influenced the directionalities of the hydrogen bonding partners in this network (Fig 8D and S10 movie), which may explain the different STD-NMR data with WT and the D285 mutant. The simulations with the GalNAcβ1–3Galα1–4Gal and the phenylurea-galabioside in complex with the WT protein converged to geometries that revealed a highly populated interaction between the ligands and N285. The ring oxygen of the GalNAc residue of the trisaccharide and the urea carbonyl oxygen of the phenylurea derivative accepted hydrogen bonds from the N285 side chain NH_2 (Fig 8B-C and S11 - S12 movies). The GalNAc HO-4 of the trisaccharide formed transient hydrogen bonds to side chain amide groups of E286 and E234, while the phenyl ring of the phenylurea ligand did not form any persistent interactions with any protein residue. The highly populated hydrogen bonds of the trisaccharide GalNAc ring oxygen and the phenylurea carbonyl oxygen to N285 could not form in the N285D mutant (Fig E-F and S13-14 movies). Instead, it was disrupted by the

formation of a water network between the D285 side chain carboxylate and the GalNAc ring oxygen of the trisaccharide (Fig 8E), while the phenylurea moiety of the phenylurea galabioside rotated away from the D285 side chain carboxylate (Fig 8F). This lack of direct hydrogen bond interactions of the GalNAc ring oxygen and urea carbonyl oxygen may at least partly explain the less efficient binding of the trisaccharide and phenyl urea derivative to the N285D mutant.

Discussion

SadP carbohydrate specificity to neutral glycolipids from lungs was studied by TLC overlay assay. The carbohydrate receptors for *S. suis* adhesion in respiratory tract and lungs have remained elusive. We studied here how SadP type P_N and P_O recognize glycolipids isolated from pig lung. The major pig lung neutral glycolipids were identified as Gb3, Gb4, the H type 2 pentaosylceramide, the Galili pentaosylceramide and Le^b and Le^y hexaosylceramides (Fig 2). In TLC overlay assay, type P_N SadP bound to Gb3 and Gb4, whereas type P_O SadP bound only to Gb3. Both SadP types showed no binding to Galα1–3Gal-containing Galili pentaosylceramide. (Fig 2AB, Table 1). Therefore, our findings suggest that globo series glycolipids are the major carbohydrate receptors for *S. suis* in pig lung. Although fucose-binding lectins have been described both in bacterial and fungal lung pathogens, no fucose-specific binding activity was found in SadP. The globo series glycolipids have been shown to be widely expressed in many tissues of pigs [26]; hence, they can potentially serve as SadP receptors for other host organs and brain capillary veins critical for *S. suis* invasive infection. We show that the binding of *S. suis* serotype 2 *sadP*-mutant to endothelial cell line was significantly reduced and binding of both the WT *S. suis* bacteria and recombinant SadP adhesin were inhibited with the galabiose-containing pigeon ovomucoid.

The oligosaccharide inhibition assays performed with both whole bacteria and recombinant adhesin suggest that the reducing end β-Glc of Gb3 is required for optimal binding [16,19]. The TLC overlay assay using purified glycolipids showed that SadP bound strongest to the P1 glycolipid (Fig 2BC and S5A Fig). The preferential binding to the P1 glycolipid might also be due to a more optimal presentation of the epitope on the longer core chain, whereas hindered presentation of binding epitope in galabiosyl ceramide might explain, why SadP did not bind to Gb2 in TLC overlay assay. The presence of P1 structure is not well known in pig,

however it was found in α1,3GalT knockout pig kidney, since this glycosyltransferase is a direct competitor of α1,4GalT [27]. This might be important for surveillance of pathogens in xenotransplantation.

The fine specificity of SadP subtypes was further analyzed with ITC and competitive inhibition assay. The ratio of K_D values (Galα1–4Gal / GalNAcβ1–3Galα1–4Gal) for type P_N SadP was 0.4 whereas for type P_O it was 0.004, which is in accordance to the corresponding hemagglutination inhibition MIC values observed with bacterial hemagglutination assays [16]. Moreover, the IC_{50} values for Galα1–4Gal and 3'-phenylurea-Galα1–4Gal are in accordance to previous hemagglutination inhibition MIC concentrations for type P_N and P_O *S. suis* [25].

The mechanism of how the two SadP subtypes differ in their recognition of Gb3, Gb4 and glycomimetic 3-phenylurea-galabiose has not been studied before. The multiple-sequence alignment of SadP showed that specific amino acids G233, E249 and N285 of type P_N in galabiose-binding domain are different compared to type P_O SadP (Fig 1A). Of these, only substitution from asparagine to aspartate at position 285 is found in all hemagglutinating type P_O adhesins. To analyze the mechanisms how SadP type P_N can bind to Gb4 terminal trisaccharide (GalNAcβ1–3Galα1–4Gal) and 3'-phenylurea-galabiose, we designed mutations to type P_N SadP and analyzed their binding to galabiose. The SadP type P_N region from H216 to D246 was swapped to the corresponding region of type P_O (to contain substitution from amino acid G to N at position 233). The binding of this mutant to galabiose was reduced compared to the wild type adhesin (S6A Fig), but was still sufficient to further analyze the oligosaccharide specificity. Deletion Δ244-246 and site-specific mutations N285D and E292Q bound also to galabiose at sufficient level (S6A Fig) allowing testing with 3'-phenylurea-derivative to compare for type-specificity. Of these mutants, only N285D lost the ability to be efficiently inhibited by 3'-phenylurea-derivative (S6B-F Fig), suggesting that N285 has an important role in interacting with the phenylurea-group. The amino acid region 216-246 including G233N substitution have possibly no significant role alone in the interaction with HO-3' substituted phenylurea-galabiose. However, G233 could still synergistically interact with phenylurea. Therefore, the N285D mutant was chosen for further studies for the type P_N binding mechanism. The WT and N285D mutant were compared for their binding to the soluble Gb4 terminal trisaccharide GalNAcβ1–3Galα1–4Gal and to globo series glycolipids Gb3 and Gb4 (Figs 5 and 6).

The results show consistently that N285 plays a specific role in Gb4 binding as demonstrated by competitive inhibition assay, ITC and liposome binding assay.

Molecular dynamics calculations were performed with the structures representing type P_N SadP(125-329) and its N285D site-specific mutant. Both proteins were analyzed with Galα1–4Gal, GalNAcβ1–3Galα1–4Gal and 3'-phenylurea-Galα1–4Gal. In accordance to the co-crystal structure (PDB id. 5boa), the galabiose HO-4', HO-6', HO-2 and HO-3 were hydrogen bonded to Y198, G233, R238, Q255 and K316. Hydrophobic interaction with the α-face of the β-galactoside stacked to W258 forming CH-π interactions. The above interactions were conserved in WT and N285 mutant. WT SadP N285 formed hydrogen bonds to GalNAc O-5 ring oxygen of GalNAcβ1–3Galα1–4Gal and to urea's carbonyl group (Fig 8B). The amino acid D285 of site-pecific mutant formed hydrogen bonds with solvent water molecules when simulated with GalNAcβ1–3Galα1–4Gal and 3'-phenylurea-Galα1–4Gal. These results together with the AlphaScreen and ITC data give us a plausible explanation for the molecular mechanism of how type P_N SadP interact with Gb4 terminal GalNAc and with phenylurea-galabiose derivative. In addition, WT SadP amino acid G233 interacts with the terminal GalNAc of Gb4 via hydrogen bond to N-Acetyl-group or to urea's -NH group (Fig 8C).

SadP does not have any sequence homologs in other galabiose-recognizing proteins, however structurally *E. coli* PapG and SadP galabiose-binding sites share some similarities. They both contain a β-sheet composed of antiparallel β-strands, which are adjacent to the galabiose-binding domain (PDB; *E. coli* 1j8r, *S. suis* 5boa). In SadP, the binding site is formed by the alpha-helix and a non-helix loop, whereas in PapG the galabiose binding site is located in the middle of two non-helix loops. Other galabiose binding proteins such as *P. aeruginosa* LecA (4yw6), *E. coli* verotoxin (1bos) and *Lyophyllum decastes* fungal lectin (4ndv) show different combining site architectures. As previously suggested, the galabiose-binding adhesin SadP from gram-positive and *E. coli* P fimbrial adhesins from gram-negative bacteria are an example of convergent evolution towards binding to the galabiose oligosaccharide. The structural similarities thus confirm this hypothesis.

Hemagglutination positive strains expressing type P_N SadP from pig and zoonotic meningitis strains belong to serotype 2 and clonal group CC1 [6,17]. *S. suis* hemagglutination type P_O strains were mostly found from serotype 4 and were isolated from lungs of strains causing pneumonia [28]. The majority of strains that

have the gene encoding type P_N SadP belongs to a distinct population consisting of systemic isolates, which were identified in a large BRaTP1T consortium functional genomic study [29]. *S. suis* strains that cause human meningitis comprise a separate clade and are thought to have evolved when the pig farming was intensified in 1920s [29]. Zoonotic *S. suis* strains as a specific population have been thought to exponentially spread to different geographical areas due to the selection of pigs that are optimal in terms of productivity. The BRaTP1T consortium study of *S. suis* genomic signatures for pig and human infections has suggested that the systemic infections are genetically determined and the genome size of highly virulent strains is reduced and enriched with virulence genes. Since the type P_N SadP adhesin gene has not been lost in strains causing systemic infections, it is tempting to speculate that the recognition of Gb4 may play a specific role in invasive infections. In a previous study by Ferrando et al. (2017), type P_N SadP (designated SadP1) present in CC1 clonal group of *S. suis* strains [17] was found to specifically adhere better to human intestinal cells (Caco-2) than to pig intestinal cells. This could indicate that type P_N SadP has specific binding preferences to human intestine, thus promoting zoonosis.

The results of the present study could have implications toward the therapeutic applications targeting SadP and *S. suis* systemic infections (summarized in Fig 9). The gene encoding SadP type P_N has a downstream homolog, which is a pseudogene (has a stop codon). It could be speculated, that the gene encoding SadP type P_N is a putatively duplicated gene, which has evolved to bind Gb4 (Figure 9A). This study shows the molecular mechanism how N285 contributes to the binding of terminal GalNAcβ1- saccharide of Gb4 by a specific interaction with GalNAc hexose ring oxygen (Figure 9BC). The analogous N285-mediated binding mechanisms to Gb4 and glycomimetic phenylurea-galabiose could be utilized in the design of therapeutics against the invasive systemic infections without disturbing the commensal *S. suis* bacteria colonizing pig upper respiratory tract.

Materials and Methods

Bacterial strains

The chromosomal DNA was isolated from type P_N and P_O *S. suis* strains as described before [6] using GelElute bacterial genomic DNA kit according to the manufacturer's instructions. *Streptococci* were grown in Todd Hewitt broth supplemented with 0.5 % yeast extract or in Columbia agar plates supplemented with 5 % sheep blood in 5 % CO_2 at 37°C and *E. coli* strain were grown in LB medium. Antibiotics used were 30 µg/ml (pET28) and 100 µg/ml ampicillin pET46EkLIC) in *E. coli* and 500 µg/ml kanamycin for *S. suis* D282Δ*SadP* mutant [6].

Escherichia coli NovaBlue (Novagen) was used for the cloning of SadP constructs and strain BL21(DE3) for expression of the adhesin.

Cloning and construction of recombinant adhesins

The galabiose binding *N*-terminal domains of SadP from hemagglutination subtypes P_N and P_O were cloned into pET46EkLIC vector as follows: The primer pairs SadPDER48 (gacgacgacaagatagaatcgctagaaccagatgtt) and SadPDER49 (gaggagaagcccggtttattcttctcaagggtaatctc) were designed to clone the 882 bp fragment of the adhesin *N*-terminal galabiose binding domain. The fragments were amplified with Phusion HotStart II DNA polymerase and were cloned into LIC-vector (LIC, ligation independent cloning) pET46EkLIC (Novagen). The ligation products were transformed into NovaBlue competent cells. This construct yielded a 33.4 kDa 6xHis-tagged fusion protein (SadP(31-328)). The sequence of *N*-terminal domains of SadP homologs were verified by sequencing with T7 promoter and T7 terminator primers. The vectors were transformed into expression strain BL21(DE3).

Site-specific mutant SadP(31-328) W258A was constructed by PCR with 5'-phosphorylated forward primer tgg aac gca tct gct ggt caa gct and reverse primer ttg aga att aaa acc att ttc. The PCR product was amplified with Phusion HotStart II DNA polymerase and the PCR fragment was ligated with T4 ligase (Promega) and transformed into Novablue competent cells. The resulting plasmid SadP(31-328)W258A-pET28a was sequenced to verify the mutation.

Synthetic gene construct and the corresponding site-specific mutants for WT SadP(125-328) type P_N were obtained from Genscript. Site-specific mutants constructed were Δ244-246 (PSAD-1), N285D (PSAD-2), E292Q (PSAD-3), N285D&Δ244-246 (PSAD-4) and H216-D246delinsDELFNRFPNKVDSTNNGDGAPFRFFNKE (PSAD-5) (replacement of aa 216-242 into corresponding sequence of type P_O of strain 6107).

Bioinformatics

To compare the distribution of SadP alleles in *S. suis* from different infections e.g. invasive, respiratory and non-clinical samples, the presence of either P_N or P_O allele was detected from 374 previously published *S. suis* isolates [29] using SRST2 software version 0.2.0 with default settings [30]. The SadP genes from *S. suis* P1/7 (AM946016.1) and 6407 (NZ_CP008921.1) were used as reference sequences for P_N and P_O, respectively. The distribution of P_N and P_O alleles in the *S. suis* phylogeny was investigated by creating a core-genome maximum-likelihood tree using Roary version 3.12.0 [31] and RAxML version 8.2.8 [32] from the 374 isolates.

Expression and purification of SadP proteins

The bacteria were grown at 30°C, 250 rpm, to an OD600 of 0.5, and the protein expression was induced with 0.2 mM IPTG for 3.5 hours. Bacteria were harvested by centrifugation with 3000 x g, at +4°C and stored at -84°C. The recombinant protein was purified with Ni-NTA affinity chromatography. Briefly, bacteria were lysed with 0.4 mg/ml hen egg lysozyme (Sigma) in 50 mM sodium phosphate buffer pH 8.0, containing 0.5 M NaCl, EDTA-free protease inhibitor cocktail (Pierce), 20 mM imidazole, 20 µg/ml deoxyribonuclease and 1 mM $MgCl_2$ on ice for 30 mins. The lysate was sonicated to further homogenize the cell debris and was centrifuged at 20000 x g, +4°C for 30 min. The filtered lysate was purified with Ni-NTA affinity chromatography using HiPrep FF column connected to Äktaprime plus, GE Healthcare at +25°C. Further purification was done with a gel filtration HiLoad 16/60 Superdex 200 column using Tris-HCl, pH 7.5, 0.15 M NaCl as running buffer. The purity of the recombinant proteins was analyzed with SDS-PAGE

chromatography. For native gel electrophoresis, the recombinant proteins were diluted to sample buffer without SDS and were separated with 8 % polyacrylamide gel.

Crystallization

SadP N285D mutant (15 mg/ml) was crystallized with the hanging-drop vapor-diffusion method. The well condition contained 1.3-1.5 M sodium citrate tribasic, 0.1 M sodium cacodylate, pH 6.5. Equal volumes of well solution and protein (2 µL+2µL) were mixed and the crystals grew at 16 °C, initially as haystacks of very thin needles. Single crystals suitable for data collection were subsequently grown by using the seeding technique. A small part of the haystack was crushed with a metallic needle in the crystallization drop and 0.2 µL were diluted in 20 µL of mother liquor to create a seeding stock. Pre-equilibrated (1-d old) crystallization drops were seeded with 0.1 µL of the seeding stock. Single crystals started to grow after ~3 days.

Data collection and crystal structure determination

Diffraction data were collected on the BioMAX beamline at MAX IV (Lund, Sweden) from a single crystal under cryogenic temperatures (100K). The crystal diffracted to 1.85 Å but the resolution was later truncated during processing to 2.05 Å owing to completeness. The crystal was found to belong to the *C*2 space group. Data processing was carried out with automated procedures in EDNA [33] and scaling was done with AIMLESS [34].

Molecular replacement with PHASER [35] was carried out to obtain initial phases using the native structure as a template. Five molecules in the crystallographic asymmetric unit were located (Matthews coefficient 2.67 $Å^3$/Da corresponding to ~53.9% solvent content). Initial building of the structure was carried out using the automated building procedure in BUCCANEER [36] using the ccp4i2 interface [37]. After the initial building that produced an almost complete structure, the refinement continued in PHENIX v.1.17.1-3660 [38] using simulated annealing at 1000K with maximum likelihood as target function. The first round of simulated annealing resulted in R_{work}/R_{free} of 0.227/0.269. Inclusion of waters and rounds of manual rebuilding using COOT [39] alternated with PHENIX refinement resulted in the final structure with R_{work}/R_{free} of

538 0.174/0.221 (Table S1). A glycerol molecule was found bound in each of the A, C, and D subunits. Two
539 glycerol molecules were located in the binding site of subunit B. The structure has been deposited to the Protein
540 Data Bank under the accession code 6YRO
541

542 **Isolation of SadP binding glycosphingolipids from porcine lung**

543 Non-acid glycosphingolipids were isolated from porcine lung as described [40]. Briefly, the lung tissue
544 was lyophilized, and then extracted in two steps in a Soxhlet apparatus with chloroform and methanol (2:1 and
545 1:9, by volume, respectively). The material obtained was subjected to mild alkaline hydrolysis and dialysis,
546 followed by separation on a silicic acid column. Acid and non-acid glycosphingolipid fractions were obtained
547 by chromatography on a DEAE-cellulose column. In order to separate the non-acid glycolipids from alkali-
548 stable phospholipids, this fraction was acetylated and separated on a second silicic acid column, followed by
549 deacetylation and dialysis. Final purifications were done by chromatographies on DEAE-cellulose and silicic
550 acid columns.
551 The total non-acid glycosphingolipid fraction (9 mg) from porcine lung was first separated on an
552 Iatrobeads (Iatrobeads 6RS-8060; Iatron Laboratories, Tokyo) column (1.0 g) and eluted with increasing
553 volumes of methanol in chloroform. Aliquots of the fractions obtained were analyzed by thin-layer
554 chromatography. Fractions that were coloured green by anisaldehyde were tested for binding of SadP using
555 the chromatogram binding assay. SadP bound to a fraction containing glycosphingolipids migrating in the tri-
556 and tetraglycosylceramide regions on thin-layer chromatograms. This fraction (1.0 mg) was further separated
557 on an Iatrobeads column (1.0 g), eluted with chloroform/methanol/water 65:25:4 (by volume), 30 x 0.5 ml,
558 followed by chloroform/methanol/water 65:25:4, 10 mi. The SadP binding triglycosylceramide was eluted in
559 fractions 12-17, and these fractions were pooled into one fraction migrating as a single band (0.2 mg, denoted
560 fraction PL-1), and fraction migrating as a double band (0.3 mg, denoted fraction PL-2) on thin-layer
561 chromatograms. In addition, a SadP tetraglycosylceramide was present in fractions 19-31, and pooling of
562 these fractions gave 0.4 mg (denoted fraction PL-4).
563

Reference glycosphingolipids

Total acid and non-acid glycosphingolipid fractions were isolated as described [40], and the individual glycosphingolipids were obtained by repeated chromatography on silicic acid columns, and by HPLC, and identified by mass spectrometry [20,41] and 1H NMR spectroscopy [42].

Thin-layer chromatography

Aluminum- or glass-backed silica gel 60 high performance thin-layer chromatography plates (Merck, Darmstadt, Germany) were used for thin-layer chromatography, and chromatographed with chloroform/methanol/water (60:35:8 by volume) as solvent system. The different glycosphingolipids were applied to the plates in quantities of 4 µg of pure glycosphingolipids, and 20-40 µg of glycosphingolipid mixtures. Chemical detection was done with anisaldehyde [43].

Radiolabeling

Aliquots of 100 µg of the different SadP protein preparations were labeled with ^{125}I by the Iodogen method according to the manufacturer's instructions (Pierce/Thermo Scientific), giving approximately 2000 cpm/µg protein.

Chromatogram binding assays

Binding of radiolabeled proteins to glycosphingolipids on thin-layer chromatograms was done as described [44]. Chromatograms with separated glycosphingolipids were dipped for 1 min in diethylether/n-hexane (1:5, by volume) containing 0.5% (w/v) polyisobutylmethacrylate (Aldrich Chern. Comp. Inc., Milwaukee, WI). After drying, the chromatograms were soaked in PBS containing 2% (w/v) bovine serum albumin, 0.1% (w/v) NaN_3 and 0.1% (w/v) Tween 20 (Solution A), for 2 h at room temperature. Thereafter the plates were incubated with ^{125}I- labeled SadP protein (l -5 x 10^6 cpm/ml) for 2 h at room temperature. After

588 washing six times with PBS, and drying, the thin-layer plates were autoradiographed for 12 h using XAR-5
589 x-ray films (Eastman Kodak, Rochester, NY).
590
591 **Microtiter well assay**

592 Binding of radiolabeled SadP to glycosphingolipids in microtiter wells was performed as described [44].
593 In short, 250 µg of pure glycosphingolipids in methanol were applied to microtiter wells (Falcon 3911, Becton
594 Dickinson Labware, Oxnard, CA). When the solvent had evaporated, the wells were blocked for 2 h at room
595 temperature with 200 µl of BSA/PBS. Thereafter, the wells were incubated for 4 h at room temperature with
596 50 µl of ^{125}I-labeled SadP (2 x 10^3 cpm/µl) diluted in BSA/PBS. After washing 6 times with PBS, the wells
597 were cut out and the radioactivity was counted in a gamma counter.
598
599 **LC-ESI/MS of native glycosphingolipids**

600 Native glycosphingolipids were analyzed by LC-ESI/MS as described [45]. Glycosphingolipids were
601 dissolved in methanol:acetonitrile in proportion 75:25 (by volume) and separated on a 200x0.150 mm column,
602 packed in-house with 5 µM polyamine II particles (YMC Europe GmbH, Dinslaken, Germany). An
603 autosampler, HTC-PAL (CTC Analytics AG, Zwingen, Switzerland) equipped with a cheminert valve (0.25
604 mm bore) and a 2 µl loop, was used for sample injection. An Agilent 1100 binary pump (Agilent technologies,
605 Palo Alto, CA) delivered a flow of 250 µl/min, which was split down in an 1/16" microvolume-T (0.15 mm
606 bore) (Vici AG International, Schenkon, Switzerland) by a 50 cm x 50 µm i.d. fused silica capillary before the
607 injector of the autosampler, allowing approximately 2-3 µl/min through the column. Samples were eluted with
608 an aqueous gradient (A:100% acetonitrile to B: 10 mM ammonium bicarbonate). The gradient (0-50% B) was
609 eluted for 40 min, followed by a wash step with 100% B, and equilibration of the column for 20 min. The
610 samples were analyzed in negative ion mode on a LTQ linear quadropole ion trap mass spectrometer (Thermo
611 Electron, San José, CA), with an IonMax standard ESI source equipped with a stainless steel needle kept at –
612 3.5 kV. Compressed air was used as nebulizer gas. The heated capillary was kept at 270 °C, and the capillary
613 voltage was –50 kV. Full scan (*m/z* 500-1800, two microscans, maximum 100 ms, target value of 30,000) was

performed, followed by data-dependent MS^2 scans (two microscans, maximun 100 ms, target value of 30.000) with normalized collision energy of 35%, isolation window of 2.5 units, activation q= 0.25 and activation time 30 ms). The threshold for MS^2 was set to 500 counts. Data acquisition and processing were conducted with Xcalibur software version 2.0.7 (Thermo Fisher Scientific). Manual assignment of glycosphingolipid sequences was done with the assistance of the Glycoworkbench tool (Version 2.1), and by comparison of retention times and MS^2 spectra of reference glycosphingolipids.

Endoglycoceramidase digestion and LC-ESI/MS

Endoglycoceramidase II from *Rhodococcus* spp. (Ito) (Takara Bio Europe S.A., Gennevilliers, France) was used for hydrolysis of glycosphingolipids. Briefly, 50 µg of glycosphingolipids were resuspended in 100 µl 0.05 M sodium acetate buffer, pH 5.0, containing 120 µg sodium cholate, and sonicated briefly. Thereafter, 1 mU of enzyme was added, and the mixture was incubated at 37°C for 48 h. The reaction was stopped by addition of chloroform/methanol/water to the final proportions 8:4:3 (by volume). The oligosaccharide-containing upper phase thus obtained was separated from detergent on a Sep-Pak QMA cartridge (Waters). The eluant containing the oligosaccharides was dried under nitrogen and under vacuum.

The glycosphingolipid-derived oligosaccharides were resuspended in 50 µl of water and analyzed by LC-ESI/MS as described [20]. The oligosaccharides were separated on a column (200 x 0.180 mm) packed in-house with 5 µm porous graphite particles (Hypercarb, Thermo-Hypersil, Runcorn, UK). An autosampler, HTC-PAL (CTC Analytics AG, Zwingen, Switzerland) equipped with a cheminert valve (0.25 mm bore) and a 2 µl loop, was used for sample injection. An Agilent 1100 binary pump (Agilent technologies, Palo Alto, CA) delivered a flow of 250 µl/min, which was split down in an 1/16" microvolume-T (0.15 mm bore) (Vici AG International, Schenkon, Switzerland) by a 50 cm x 50 µm i.d. fused silica capillary before the injector of the autosampler, allowing approximately 2-3 µl/min through the column. The oligosaccharides (3 µl) were injected on to the column and eluted with an acetonitrile gradient (A: 10 mM ammonium bicarbonate; B: 10 mM ammonium bicarbonate in 80% acetonitrile). The gradient (0-45% B) was eluted for 46 min, followed by

a wash step with 100% B, and equilibration of the column for 24 min. A 30 cm x 50 µm i.d. fused silica capillary was used as transfer line to the ion source.

The oligosaccharides were analyzed in negative ion mode on an LTQ linear quadrupole ion trap mass spectrometer (Thermo Electron, San José, CA). The IonMax standard ESI source on the LTQ mass spectrometer was equipped with a stainless-steel needle kept at –3.5 kV. Compressed air was used as nebulizer gas. The heated capillary was kept at 270 °C, and the capillary voltage was –50 kV. Full-scan (*m/z* 380-2 000, 2 microscans, maximum 100 ms, target value of 30 000) was performed, followed by data dependent MS^2 scans of the three most abundant ions in each scan (2 microscans, maximum 100 ms, target value of 10 000). The threshold for MS^2 was set to 500 counts. Normalized collision energy was 35%, and an isolation window of 3 u, an activation q = 0.25, and an activation time of 30 ms, was used. Data acquisition and processing were conducted with Xcalibur software (Version 2.0.7).

Manual assignment of glycan sequences was done on the basis of knowledge of mammalian biosynthetic pathways, with the assistance of the Glycoworkbench tool (Version 2.1), and by comparison of retention times and MS^2 spectra of oligosaccharides from reference glycosphingolipids [20].

S. suis cell binding assay

EA.hy926 cells were maintained and grown in DMEM, 10 % FCS medium at 37°C, 5 % CO_2. For bacterial binding assay the cells were detached with Trypsin-EDTA, counted and 15 000 cells/well added into round glass coverslips in 24 well-plates. Cells were grown for 24 - 48 h to subconfluency.

S. suis D282 WT strain and D282-Δ*sadP* were grown in THY overnight at 37°C, 5 % CO_2. Bacteria were diluted 1/20 into prewarmed 37°C THY and were grown to OD550 of 0.2 and were diluted 1/100 into prewarmed DMEM, 10 % FCS without antibiotics. 500 µl of bacterial dilution was pipetted into the wells (MOI 100:1) and the plate was centrifuged with 800 x g, 15 min at 20°C.

The plate was incubated at 37°C for 1 h. The wells were washed 4 x 1000 µl of PBS. The cells were stained with DiffQuick kit, washed and the coverslips were mounted on glass slides with Permount.

664 The bacterial binding was quantitated by microscopy with 100 x objective with immersion oil. The
665 bound bacteria were enumerated by counting two wells for each sample. The results were expressed as average
666 of bacteria / optical field.

667 For flow cytometry, N-terminal domain of SadP was labelled with FITC (Sigma-Aldrich) in 0.2 M
668 borate buffer, pH 8.0, 0.16 M NaCl (50:1 molar ratio of FITC/SadP, 83 nmol of SadP and 1.7 µmol of FITC)
669 and the labelling was stopped with Tris-buffer. The labelled SadP was purified from the free FITC with PD-
670 10 (GE Healthcare) desalting column. The EA.hy926 cells were seeded into 6 well culture dishes (1 x 10^5
671 cells/well) and were grown for 48 h. The cells were washed with DMEM and were incubated with 400 ng/ml
672 of labelled SadP with or without 10 µg/ml pigeon ovomucoid. After binding, the wells were washed with
673 phosphate Buffered Saline (PBS, 0.15 M NaCl, 2.7 mM KCl, 8.1 mM Na_2HPO_4, 1.5 mM KH_2PO_4). and were
674 fixed with 2 % (w/v) paraformaldehyde in PBS for 15 min. The cells were washed twice with PBS and the
675 cells were scraped of the wells and suspended into the PBS. 10 000 cells were analyzed for SadP binding with
676 FACSCalibur.
677

678 **Amplified luminescent proximity homogeneous assay (AlphaScreen)**

679 The AlphaScreen assay was optimized as described before [19]. Briefly, the assay was performed using
680 AlphaScreen Streptavidin Donor beads and NiNTA Acceptor beads (PerkinElmer). The molar concentrations
681 of galabiose-containing biotinylated ovomucoid (receptor) and adhesin were optimized by finding the hook
682 point for the interaction by setting up a matrix of proteins in 96 well AlphaPlates (Perkin Elmer) in 10 mM
683 Tris-HCl, pH 7.5, 0.15 M NaCl, 0.2% BSA, 0.05 % Tween 20 0.2% (TBST-0.2%BSA). For the optimized
684 assay dilutions of 5 µl of the His-tagged adhesin and 5 µl of biotinylated ovomucoid were pipetted into the
685 wells and the plates were centrifuged for 1 min, 1000 x g. The plates were incubated at +25°C for 1 hr. This
686 was followed by addition of Ni-NTA- beads (20 µg/ml) and incubation for 1.5 hrs. Finally, streptavidin donor
687 beads were added (20 µg/ml) and the mixtures were incubated for 30 mins and were then measured with the
688 Ensight multimode reader (Perkin Elmer) using excitation wavelength of 680 nm with donor beads and
689 measurement of emission wavelength of 615 nm from AlphaLISA anti-HIS acceptor beads. For inhibition
690 assays the oligosaccharides, whose structures have been described before [25] or depicted in Figure 4 for

TMSEt- glycosides of GalNAcβ1–3Galα1–4Gal and 3Galα1–4Gal, were diluted into TBST-0.2%BSA buffer and were mixed with the His-tagged adhesin and biotinylated ovomucoid. The binding was measured as described above. The binding inhibition data was fitted using Prism with settings of log(inhibitor) vs. response slope (four parameters).

Isothermal titration calorimetry

SadP-D282(31-328) (P_N), SadP-6107(31-328) (P_O), SadP(125-329) type P_N and site-specific mutant SadP(125-328)N285D were desalted into PBS using PD-10 desalting column (GE Healtcare). The synthetic oligosaccharides were diluted to the same buffer. 0.1 - 0.2 µM of SadP proteins in a 350 µl vessel was titrated with 1.5 - 2 mM solutions of galabiose oligosaccharides using MicroCal (Malvern). The protein solution was stirred with 750 rpm at 25°C and 16 injections of a volume of 2.49 µl were injected at 180 s intervals. The data from single determinations was analyzed with Origin.

Preparation of liposomes and SadP binding assay

Vesicles were prepared as described before [46]. Briefly, POPC (1-palmitoyl-2-oleoyl-glycero-3-phosphocholine, Avanti Polar lipids), cholesterol and glycolipids were dissolved and mixed into the chloroform : methanol (2:1, vol/vol) to contain 30 % cholesterol and 2 mM glycolipids. The solvent was evaporated and the lipid film was suspended for 30 min at 60 °C in 10 mM Tris-Cl, 140 mM NaCl buffer. The lipid-buffer suspension was briefly vortexed followed by the extrusion procedure (Avanti mini extruder using 0.1 µm polycarbonate membranes filter, (Avanti Polar Lipids, Alabaster, AL, USA)) to form large unilamellar vesicles.

PVDF membrane was wetted (wetting in 100 % MeOH, washing 4 x 5 min MilliQ water) and was overlaid onto wet Whatman filter paper. Liposomes were serially diluted 1/10 into Tris-buffered saline and 2 µl of liposomes containing 2 mM, 0.2 mM and 0.02 mM of glycolipid was pipetted onto the membrane and the membrane was not allowed to dry during the pipetting. The membrane was saturated with 2 % BSA (w/v) in TBS for 1 h at 20°C and was incubated with 10 µg/ml recombinant SadP for 2 h at 20°C. The membrane

was washed 4 x 5 min with TBS and the bound SadP was detected with 1:10000 dilution of anti-His primary antibody (Sigma) and 1:20000 dilution of HRP-labelled secondary rabbit anti-mouse antibody (DakoCytomation). The membrane was incubated with ECL substrate (WesternBright Quantum, Labtech) and the SadP binding was imaged with Fuji LAS-4000.

STD-NMR

STD-NMR measurements were carried out on a Bruker AVANCE III HD spectrometer (Bruker BioSpin GmbH, Rheinstetten, Germany) operating at 600.13 MHz, equipped with a nitrogen-cooled triple-channel TCI inverse CryoProbe™. The pulse sequence used for the experiments was the stddiffesgp provided by Bruker. A 1x PBS buffer with a pH of 7.45 with 10% D_2O, containing 50 µM protein and 2500 µM Gb3 trisaccharide was used for the experiments. The on-resonance pulse was set to the methyl groups at 0.9 ppm and the off-resonance pulse was set at 20 ppm. A saturation time of 2 s was used and the experiments were carried out at 313 K to somewhat improve the weak signals, likely resulting from slow k_{off}. A blank experiment with only Gb3 and no protein was done to rule out any self-STD.

Molecular dynamics simulations

Molecular dynamics simulations were performed with the OPLS3 force field in Desmond (Schrödinger Release 2019-4: Desmond Molecular Dynamics System, D. E. Shaw Research, New York, NY, 2017; Maestro-Desmond Interoperability Tools, Schrödinger, New York, NY, 2017) using default settings except for the length of the simulation. Simulations were performed with periodic boundary conditions using orthorhombic simulation boxes with SPC water model. Counter ions were used to neutralize each other. Starting conformations of ligands in complex with SadP (pdb id 5BOA) were built by manually placing ligand galabiose residues in an identical position to that in the crystal structure (pdb id 5BOA). Complexes with the mutants were generated by exchanging N285 for D285. The complexes were then subjected to 100 ns molecular dynamics simulations. The complex of the phenylurea derivative with the N285D mutant was not

742 stable during the 100 ns simulations. Therefore, light constraints (1 kcal·mol^{-1}·Å^{-1}) on the protein secondary
743 structures were applied. Molecular images were generated using PyMOL v2.30 (Schrodinger LLC).
744

745 Acknowledgements

746 The synthetic glycolipid Galα1–4Galβ1–O-bis-(SO_2-$C_{16}H_{33}$)$_2$ was a kind gift from Professor Göran
747 Magnusson, Lund University, Sweden. ACP thanks Noushin Madani for help during crystallographic data
748 collection. Infrastructure support from Biocenter Finland is acknowledged.
749

750 References

751

752 1. Pizarro-Cerda J, Cossart P. Bacterial adhesion and entry into host cells. Cell. 2006;124: 715–727.
753 doi:10.1016/j.cell.2006.02.012
754 2. Weinbaum S, Tarbell JM, Damiano ER. The Structure and Function of the Endothelial Glycocalyx
755 Layer. Annu Rev Biomed Eng. 2007;9: 121–67. doi:10.1146/annurev.bioeng.9.060906.151959
756 3. Lingwood CA, Binnington B, Manis A, Branch DR. Globotriaosyl ceramide receptor function - where
757 membrane structure and pathology intersect. FEBS Lett. 2010;584: 1879–1886.
758 doi:10.1016/j.febslet.2009.11.089
759 4. Stromberg N, Marklund BI, Lund B, Ilver D, Hamers A, Gaastra W, et al. Host-specificity of
760 uropathogenic *Escherichia coli* depends on differences in binding specificity to Gal alpha 1-4Gal-
761 containing isoreceptors. EMBO J. 1990;9: 2001–2010.
762 5. Chemani C, Imberty A, de Bentzmann S, Pierre M, Wimmerova M, Guery BP, et al. Role of LecA and
763 LecB lectins in *Pseudomonas aeruginosa*-induced lung injury and effect of carbohydrate ligands. Infect
764 Immun. 2009;77: 2065–2075. doi:10.1128/IAI.01204-08
765 6. Kouki A, Haataja S, Loimaranta V, Pulliainen ATAT, Nilsson UJUJJ, Finne J. Identification of a novel
766 streptococcal adhesin P (SadP) protein recognizing galactosyl-α1-4-galactose-containing

glycoconjugates: Convergent evolution of bacterial pathogens to binding of the same host receptor. J Biol Chem. 2011;286: 38854–38864. doi:10.1074/jbc.M111.260992

7. Rello J, Parisella FR, Perez A. Alternatives to antibiotics in an era of difficult-to-treat resistance: new insights. Expert Review of Clinical Pharmacology. 2019. pp. 12(7):635-642. doi:10.1080/17512433.2019.1619454

8. Alves M, Ferreira IFR, Dias J, Teixeira V, Martins A, Pintado M. A review on antimicrobial activity of mushroom (basidiomycetes) extracts and isolated compounds. Planta Medica. 2012. pp. 78(16):1707-1718. doi:10.1055/s-0032-1315370

9. Bernardi A, Jimenez-Barbero J, Casnati A, Castro C De, Darbre T, Fieschi F, et al. Multivalent glycoconjugates as anti-pathogenic agents. Chem Soc Rev. 2013;42: 4709–4727. doi:10.1039/c2cs35408j [doi]

10. Cozens D, Read RC. Anti-adhesion methods as novel therapeutics for bacterial infections. Expert Rev Anti Infect Ther. 2012;10: 1457–1468. doi:10.1586/eri.12.145

11. Zhang B, Ku X, Yu X, Sun Q, Wu H, Chen F, et al. Prevalence and antimicrobial susceptibilities of bacterial pathogens in Chinese pig farms from 2013 to 2017. Sci Rep. 2019;9: 9908. doi:10.1038/s41598-019-45482-8

12. Vötsch D, Willenborg M, Weldearegay YB, Valentin-Weigand P. *Streptococcus suis* - The "two faces" of a pathobiont in the porcine respiratory tract. Frontiers in Microbiology. 2018. p. 9:480. doi:10.3389/fmicb.2018.00480

13. Fittipaldi N, Segura M, Grenier D, Gottschalk M. Virulence factors involved in the pathogenesis of the infection caused by the swine pathogen and zoonotic agent *Streptococcus suis*. Future Microbiol. 2012;7: 259–279. doi:10.2217/fmb.11.149; 10.2217/fmb.11.149

14. Baums CG, Valentin-Weigand P. Surface-associated and secreted factors of *Streptococcus suis* in epidemiology, pathogenesis and vaccine development. Anim Health Res Rev. 2009;10: 65–83. doi:10.1017/S146625230999003X; 10.1017/S146625230999003X

15. Kouki A, Pieters RJRJ, Nilsson UJUJ, Loimaranta V, Finne J, Haataja S. Bacterial Adhesion of *Streptococcus suis* to Host Cells and Its Inhibition by Carbohydrate Ligands. Biology (Basel). 2013;2: 918–935. doi:10.3390/biology2030918

16. Haataja S, Tikkanen K, Nilsson U, Magnusson G, Karlsson K-AA, Finne J. Oligosaccharide-receptor interaction of the Gal alpha 1-4Gal binding adhesin of *Streptococcus suis*. Combining site architecture and characterization of two variant adhesin specificities. J Biol Chem. 1994;269: 27466–27472.

17. Ferrando ML, Willemse N, Zaccaria E, Pannekoek Y, Van Der Ende A, Schultsz C. Streptococcal Adhesin P (SadP) contributes to *Streptococcus suis* adhesion to the human intestinal epithelium. PLoS One. 2017;12: e0175639. doi:10.1371/journal.pone.0175639

18. Kong D, Chen Z, Wang J, Lv Q, Jiang H, Zheng Y, et al. Interaction of factor H-binding protein of *Streptococcus suis* with globotriaosylceramide promotes the development of meningitis. Virulence. 2017;8: 1290–1303. doi:10.1080/21505594.2017.1317426

19. Haataja S, Verma P, Fu O, Papageorgiou AC, Pöysti S, Pieters RJ, et al. Rationally Designed Chemically Modified Glycodendrimer Inhibits *Streptococcus suis* Adhesin SadP at Picomolar Concentrations. Chem - A Eur J. 2018;24: 1905–1912. doi:10.1002/chem.201704493

20. Karlsson H, Halim A, Teneberg S. Differentiation of glycosphingolipid-derived glycan structural isomers by liquid chromatography/mass spectrometry. Glycobiology. 2010. doi:10.1093/glycob/cwq070

21. Chai W, Lawson AM, Piskarev V. Branching pattern and sequence analysis of underivatized oligosaccharides by combined MS/MS of singly and doubly charged molecular ions in negative-ion electrospray mass spectrometry. J Am Soc Mass Spectrom. 2002. doi:10.1016/S1044-0305(02)00363-X

22. Robbe C, Capon C, Coddeville B, Michalski JC. Diagnostic ions for the rapid analysis by nano-electrospray ionization quadrupole time-of-flight mass spectrometry of O-glycans from human mucins. Rapid Commun Mass Spectrom. 2004. doi:10.1002/rcm.1352

23. Suzuki N, Khoo KH, Chen HC, Johnson JR, Lee YC. Isolation and characterization of major glycoproteins of pigeon egg white: ubiquitous presence of unique N-glycans containing Galalpha1-4Gal. J Biol Chem. 2001;276: 23221–23229. doi:10.1074/jbc.M101379200

24. Nilsson U, Ray AK, Magnusson G. Synthesis of the globotetraose tetrasaccharide and terminal tri- and di-saccharide fragments. Carbohydr Res. 1994. doi:10.1016/0008-6215(94)90010-8

25. Ohlsson J, Larsson A, Haataja S, Alajaaski J, Stenlund P, Pinkner JSS, et al. Structure-activity

relationships of galabioside derivatives as inhibitors of *E. coli* and *S. suis* adhesins: nanomolar inhibitors of S. suis adhesins. OrgBiomolChem. 2005;3: 886–900. doi:10.1039/b416878j

26. Steil D, Bonse R, Meisen I, Pohlentz G, Vallejo G, Karch H, et al. A topographical atlas of shiga toxin 2e receptor distribution in the tissues of weaned piglets. Toxins (Basel). 2016. doi:10.3390/toxins8120357

27. Diswall M, Ångström J, Karlsson H, Phelps CJ, Ayares D, Teneberg S, et al. Structural characterization of α1,3-galactosyltransferase knockout pig heart and kidney glycolipids and their reactivity with human and baboon antibodies. Xenotransplantation. 2010. doi:10.1111/j.1399-3089.2009.00564.x

28. Kurl DNN, Haataja S, Finne J. Hemagglutination activities of group B, C, D, and G streptococci: Demonstration of novel sugar-specific cell-binding activities in *Streptococcus suis*. Infect Immun. 1989;57: 384–389.

29. Weinert LA, Chaudhuri RR, Wang J, Peters SE, Corander J, Jombart T, et al. Genomic signatures of human and animal disease in the zoonotic pathogen *Streptococcus suis*. Nat Commun. 2015. doi:10.1038/ncomms7740

30. Inouye M, Dashnow H, Raven LA, Schultz MB, Pope BJ, Tomita T, et al. SRST2: Rapid genomic surveillance for public health and hospital microbiology labs. Genome Med. 2014. doi:10.1186/s13073-014-0090-6

31. Page AJ, Cummins CA, Hunt M, Wong VK, Reuter S, Holden MTG, et al. Roary: Rapid large-scale prokaryote pan genome analysis. Bioinformatics. 2015. doi:10.1093/bioinformatics/btv421

32. Stamatakis A. RAxML version 8: A tool for phylogenetic analysis and post-analysis of large phylogenies. Bioinformatics. 2014. doi:10.1093/bioinformatics/btu033

33. Monaco S, Gordon E, Bowler MW, Delagenière S, Guijarro M, Spruce D, et al. Automatic processing of macromolecular crystallography X-ray diffraction data at the ESRF. J Appl Crystallogr. 2013. doi:10.1107/S0021889813006195

34. Evans PR, Murshudov GN. How good are my data and what is the resolution? Acta Crystallogr Sect D Biol Crystallogr. 2013. doi:10.1107/S0907444913000061

35. McCoy AJ, Grosse-Kunstleve RW, Adams PD, Winn MD, Storoni LC, Read RJ. Phaser crystallographic software. J Appl Crystallogr. 2007. doi:10.1107/S0021889807021206

851 36. Cowtan K. The Buccaneer software for automated model building. 1. Tracing protein chains. Acta
852 Crystallogr Sect D Biol Crystallogr. 2006. doi:10.1107/S0907444906022116
853 37. Potterton L, Agirre J, Ballard C, Cowtan K, Dodson E, Evans PR, et al. CCP 4 i 2: The new graphical
854 user interface to the CCP 4 program suite. Acta Crystallogr Sect D Struct Biol. 2018.
855 doi:10.1107/S2059798317016035
856 38. Adams PD, Afonine P V., Bunkóczi G, Chen VB, Davis IW, Echols N, et al. PHENIX: A
857 comprehensive Python-based system for macromolecular structure solution. Acta Crystallogr Sect D
858 Biol Crystallogr. 2010. doi:10.1107/S0907444909052925
859 39. Emsley P, Cowtan K. Coot: Model-building tools for molecular graphics. Acta Crystallogr Sect D Biol
860 Crystallogr. 2004. doi:10.1107/S0907444904019158
861 40. Karlsson KA. Preparation of Total Nonacid Glycolipids for Overlay Analysis of Receptors for Bacteria
862 and Viruses and for Other Studies. Methods Enzymol. 1987. doi:10.1016/0076-6879(87)38018-8
863 41. Samuelsson BE, Pimlott W, Karlsson KA. Mass spectrometry of mixtures of intact glycosphingolipids.
864 Methods Enzymol. 1990. doi:10.1016/0076-6879(90)93442-N
865 42. Koerner TAW, Prestegard JH, Demou PC, Yu RK. High-Resolution Proton NMR Studies of
866 Gangliosides. 1. Use of Homonuclear Two-Dimensional Spin-Echo J-Correlated Spectroscopy for
867 Determination of Residue Composition and Anomeric Configurations. Biochemistry. 1983.
868 doi:10.1021/bi00280a014
869 43. E S. Dünnschicht-Chromatographie. Berlin: Springer-Verlag; 1962.
870 44. Jansson L, Ångström J, Lebens M, Imberty A, Varrot A, Teneberg S. Carbohydrate binding specificities
871 and crystal structure of the cholera toxin-like B-subunit from *Citrobacter freundii*. Biochimie. 2010.
872 doi:10.1016/j.biochi.2010.02.010
873 45. Johansson MM, Dedic B, Lundholm K, Branzell FB, Barone A, Benktander J, et al. Characterization
874 of moose intestinal glycosphingolipids. Glycoconj J. 2015. doi:10.1007/s10719-015-9604-8
875 46. Halling KK, Ramstedt B, Nyström JH, Slotte JP, Nyholm TKM. Cholesterol interactions with fluid-
876 phase phospholipids: Effect on the lateral organization of the bilayer. Biophys J. 2008.
877 doi:10.1529/biophysj.108.133744
878 47. Robert X, Gouet P. Deciphering key features in protein structures with the new ENDscript server.

879 Nucleic Acids Res. 2014. doi:10.1093/nar/gku316

880

881

Tables

Table 1.

Table 1. Binding of SadP to glycosphingolipids on thin-layer chromatograms

No. Trivial name	Structure	SadP type P_N/P_O	Source
1. Galabiaosylcer (Gb2)	Galα1–4Galβ–O–Cer	-	Human meconium
2. Galabiaosylcer (Gb2-S)	Galα1–4Galβ1–O–*bis*-(SO_2-$C_{16}H_{33}$)$_2$	-	Synthetic
3. Isoglobotri (iGb3)	Galα1–3Galβ1–4Glcβ1–O–Cer	+/-	Cat intestine
4. Globotri (Gb3)	Galα1–4Galβ1–4Glcβ1–O–Cer	+++/+++	Human erythrocytes
5. Globotetra (Gb4)	GalNAcβ1–3Galα1–4Galβ1–4Glcβ1–O–Cer	+/-	Human erythrocytes
6. Forssman	GalNAcα1–3GalNAcβ1–3Galα1–4Galβ1–4Glcβ1–O–Cer	+/-	Dog intestine
7. para-Forssman	GalNAcβ1–3GalNAcβ1–3Galα1–4Galβ1–4Glcβ1–O–Cer	-	Human erythrocytes
8. P1	Galα1–4Galβ1–4GlcNAcβ1–3Galβ1–4Glcβ1–O–Cer	+++/+++	Human erythrocytes
9. H type 4/Globo H hexa	Fucα1–2Galβ1–3GalNAcβ1–3Galα1–4Galβ1–4Glcβ1–O–Cer	-	Pig intestine
10. H type 2 penta	Fucα1–2Galβ1–4GlcNAcβ1–3Galβ1–4Glcβ1–O–Cer	-	Pig lung
11. Galili penta	Galα1–3Galβ1–4GlcNAcβ1–3Galβ1–4Glcβ1–O–Cer	-	Pig lung
12. Le^b hexa	Fucα1–2Galβ1–3(Fucα1–4)GlcNAcβ1–3Galβ1–4Glcβ1–O–Cer	-	Pig lung
13. Le^y hexa	Fucα1–2Galβ1–4(Fucα1–3)GlcNAcβ1–3Galβ1–4Glcβ1–O–Cer	-	Pig lung
14. A type 2 hexa	Galα1–3(Fucα1–2)Galβ1–4GlcNAcβ1–3Galβ1–4Glcβ1–O–Cer	-	Pig erythrocytes
15. A type 4/Globo A hepta	GalNAcα1–3(Fucα1–2)Galβ1–3GalNAcβ1–3Galα1–4Galβ1–4Glcβ1–O–Cer	-	Pig intestine

[a] Binding is defined as follows: +++ denotes a highly reproducible binding of SadP type P_N/P_O when 4 μg of the glycosphingolipid was applied on the thin-layer chromatogram, while + denotes an occasional binding, and - denotes no binding even at 4 μg.

Figures

Fig 1.

A.

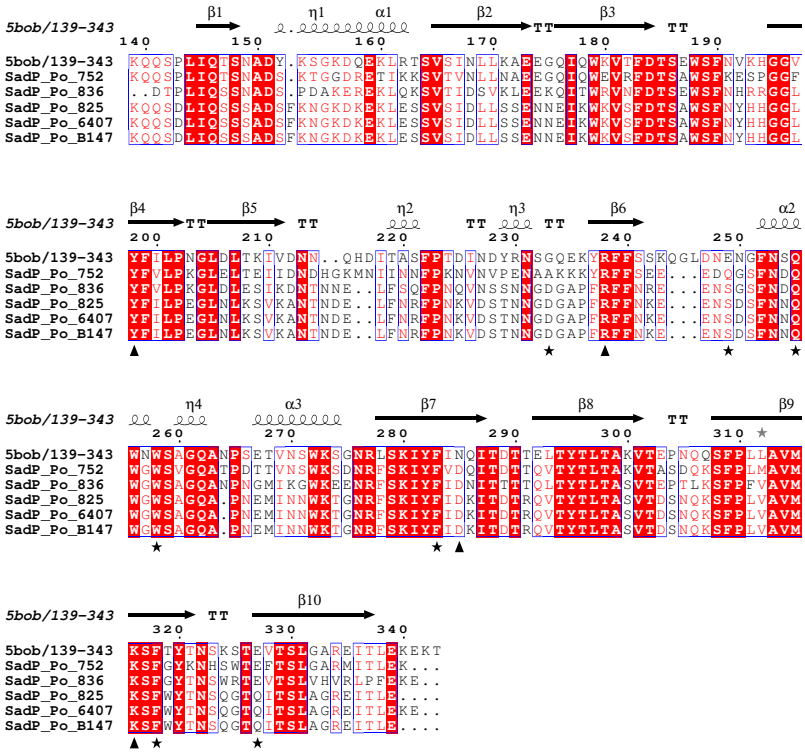

B

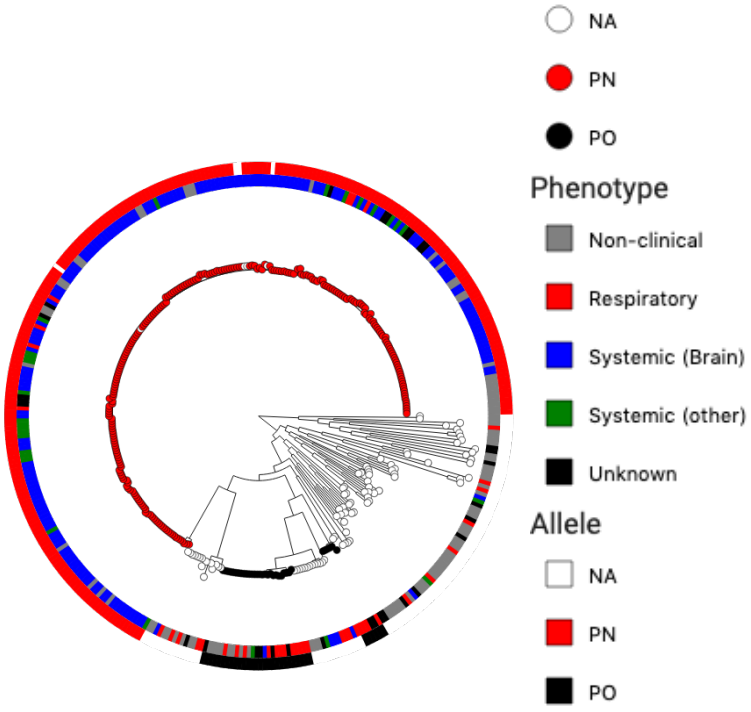

Fig 2.

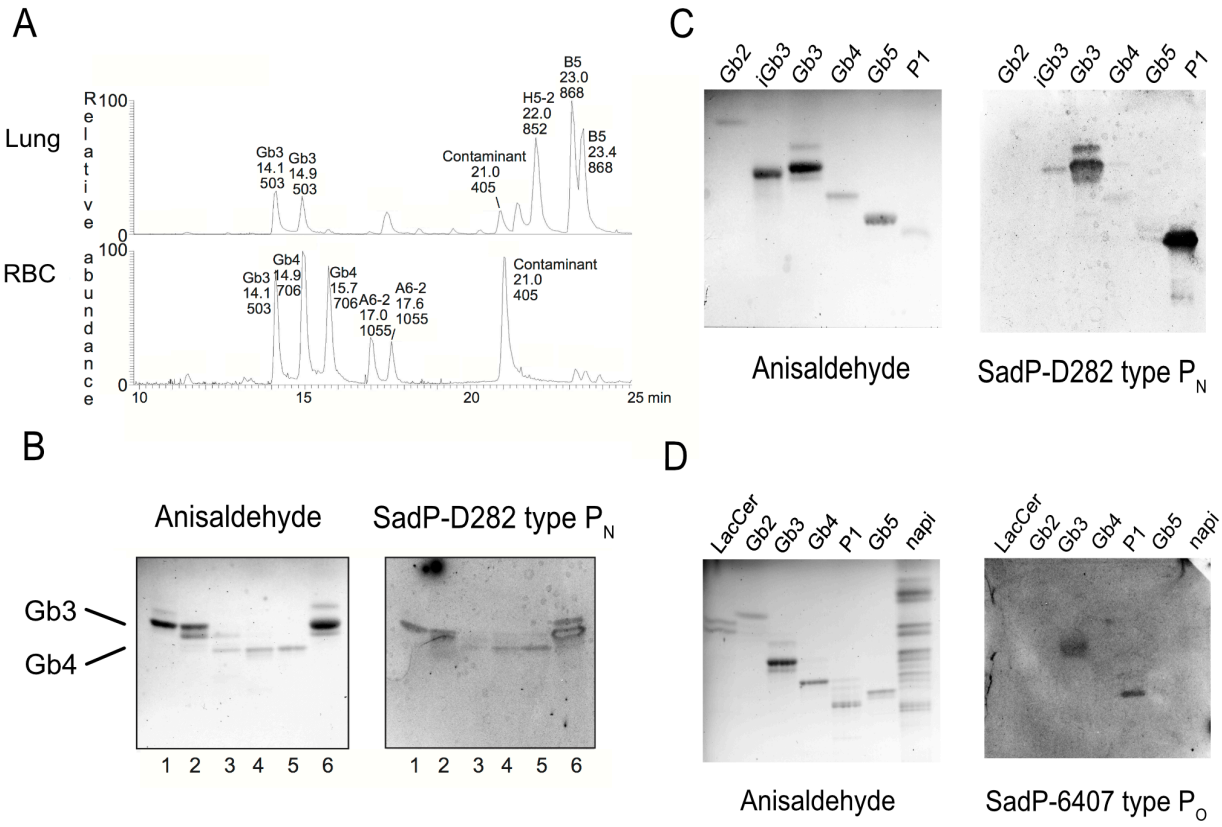

Fig. 3.

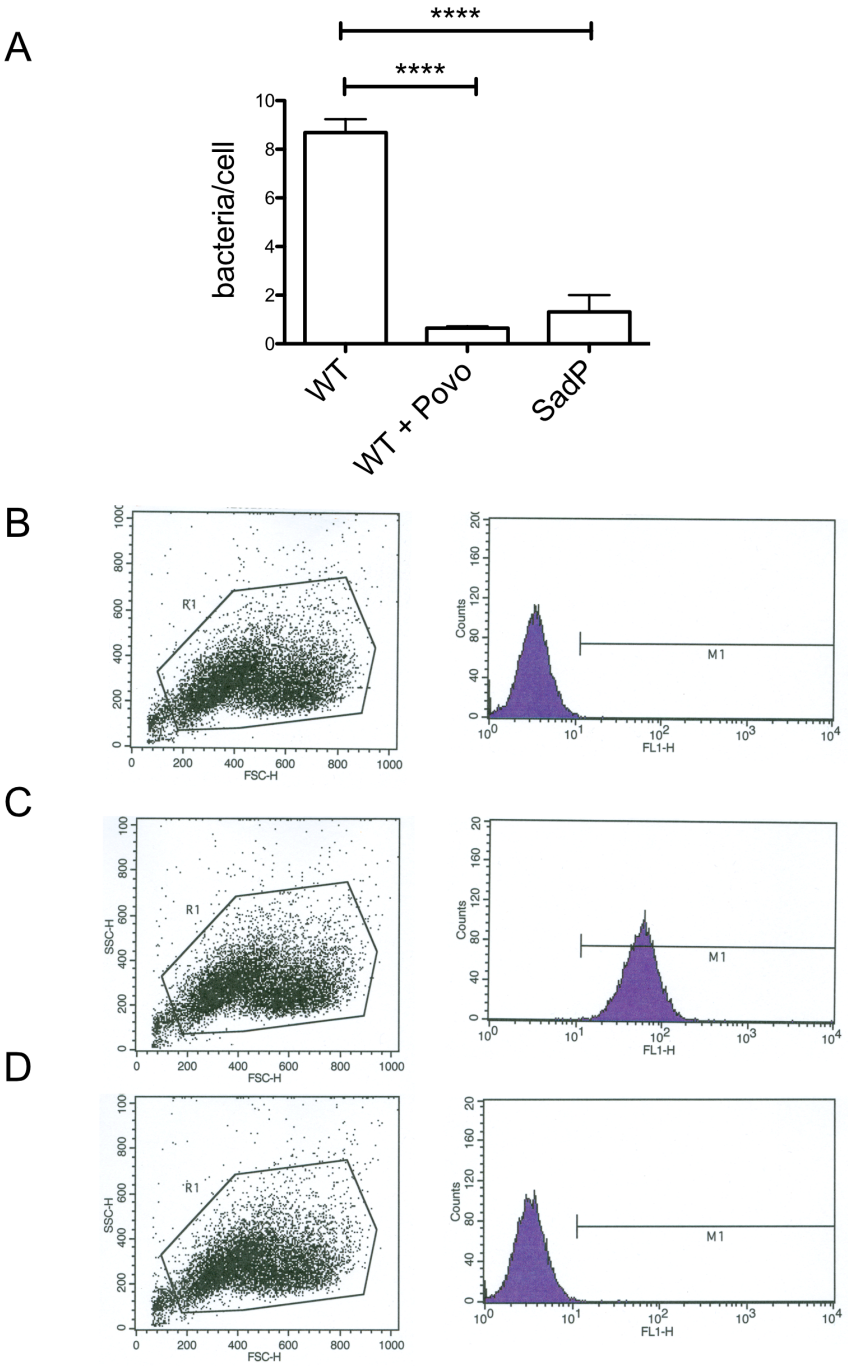

Fig 4.

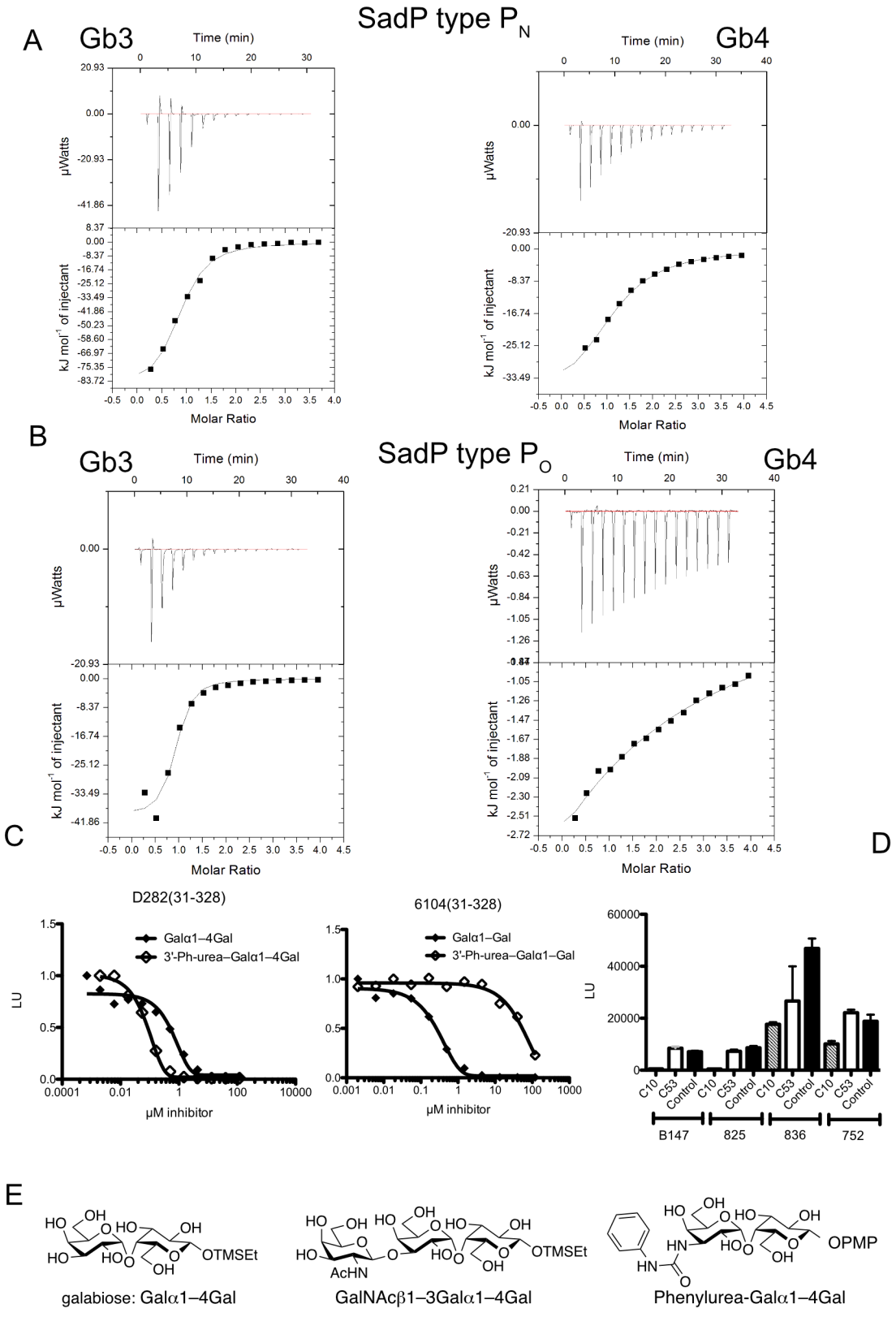

Fig 5.

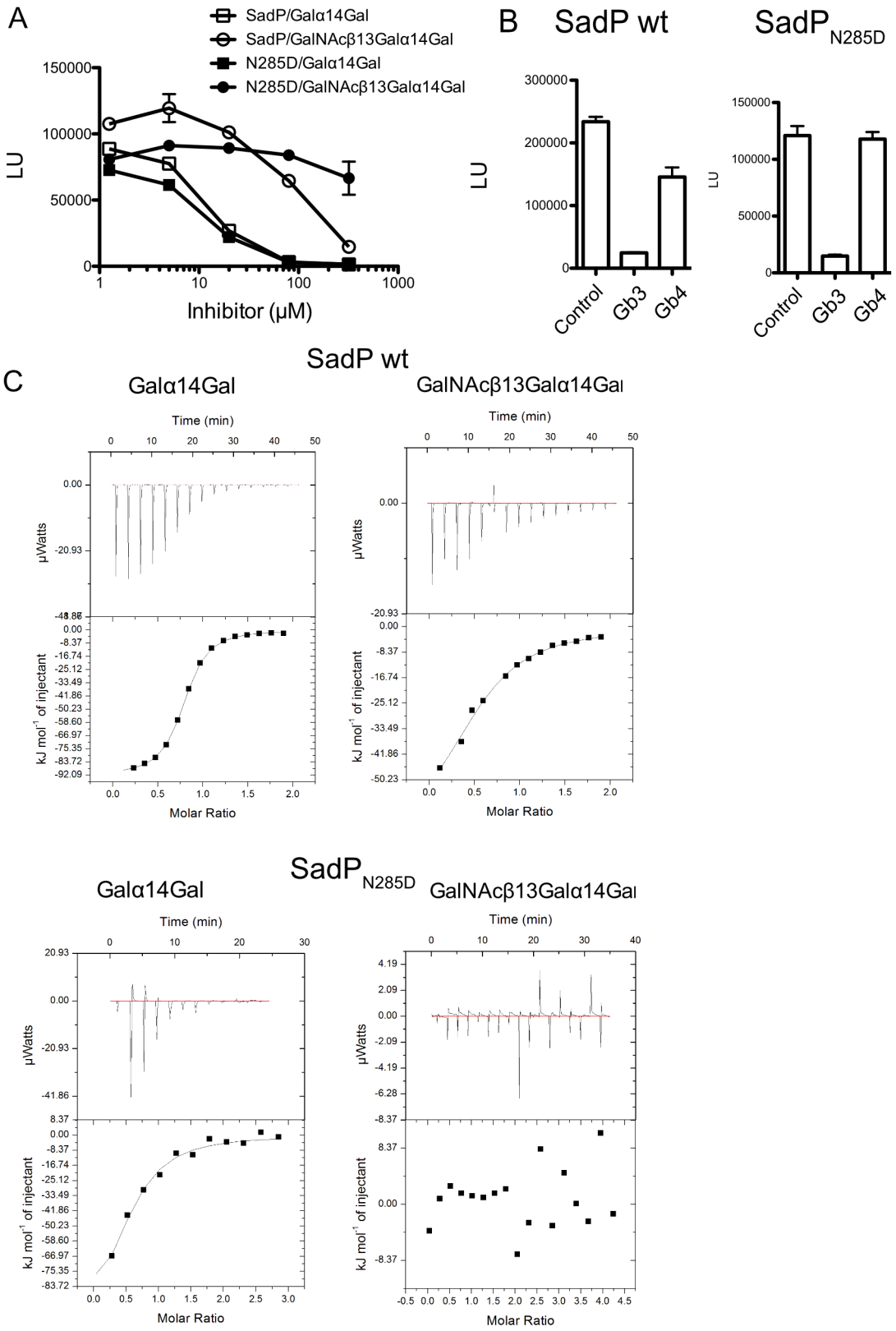

Fig 6.

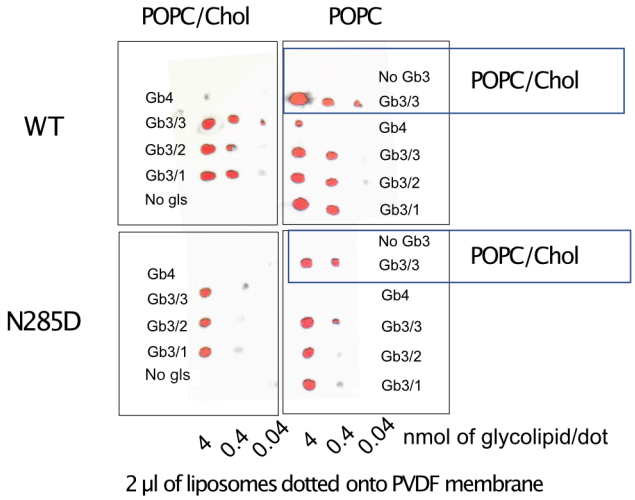

Fig 7.

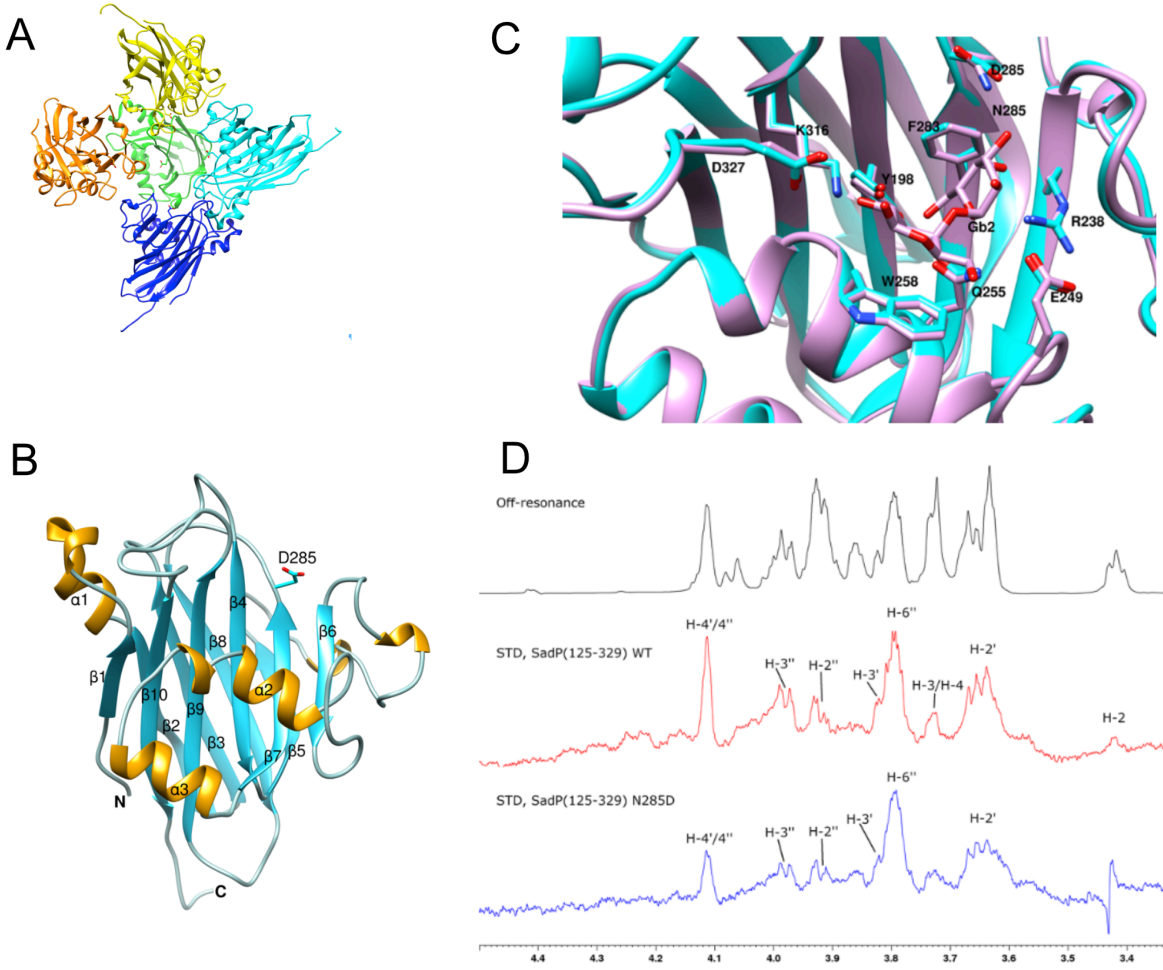

Fig 8.

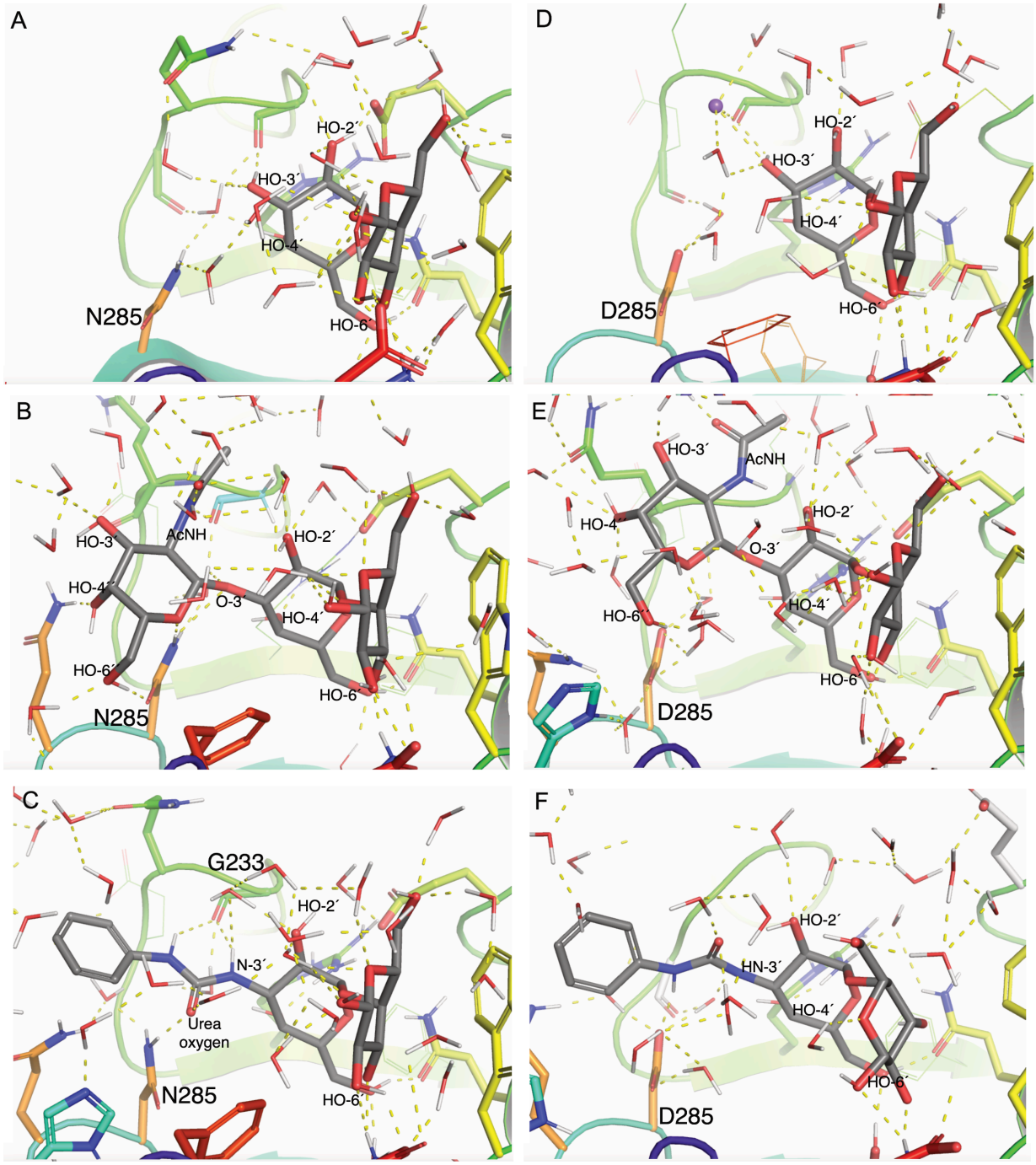

Fig 9.

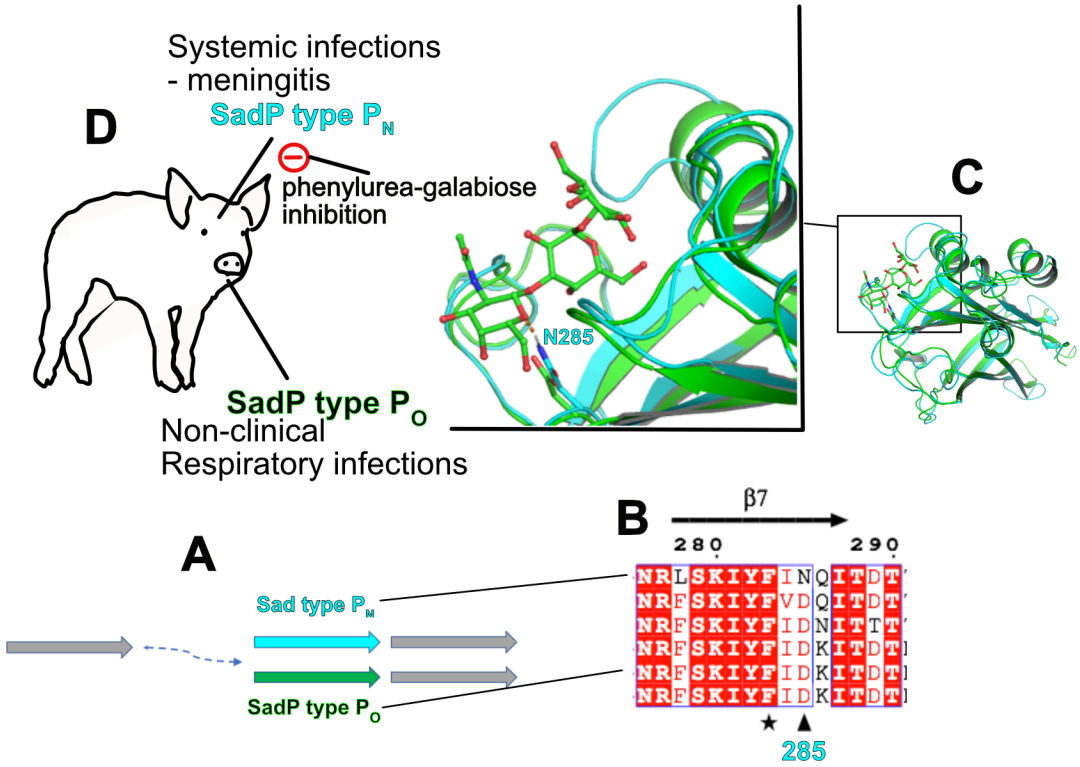

Figure legends

Fig 1. Homology of SadP types P_N and P_O galabiose-binding domains and their distribution in systemic, respiratory and non-clinical *S. suis* isolates. A. Multiple alignment of SadP galabiose binding domains of type P_N and type P_O strains. Conserved amino acids are shown in shaded red rectangles and white letters. Residues with >70% similarity according to their physicochemical properties are framed in white background and shown with red letters. Residues involved in hydrogen-bond formation with galabiose (Galα1–4Gal) are shown with (▲) and those involved in hydrophobic interactions with a star (★). Residues 139-343 of SadP are included as found in the crystal structure (pdb id 5BOB). Secondary structure elements are shown on the top. Figure was created with ESpript [47]. **B. Distribution of SadP type P_N and P_O alleles in *S. suis* clinical and non-clinical isolates.** Maximum-likelihood core genome phylogeny of 374 *S. suis* isolates from Weinert et al. 2015. The phylogeny was run with RAxML using SNP sites. The nucleotide substitution model used was GTR GAMMA. Tips of the tree are coloured according to the SadP allele detected with SRST2. NA means that with the default parameters neither allele was detected. The inner circle shows the phenotype according to Weinert et al. 2015. Grey non-clinical, red respiratory, blue systemic (brain), green systemic (other) and black unknown. The outer circle is coloured according to the SadP allele detected with SRST2 with the same colours as the tree tips. White NA, red P_N and black P_O.

Fig 2. Different glycolipid binding specificities of SadP type P_N from systemic *S. suis* strains and type P_O SadP from respiratory strains towards pig lung glycolipids and purified globo series glycolipids . A. Comparison of the total non-acid glycosphingolipid fractions from porcine lung and erythrocytes. Base peak chromatogram from LC-ESI/MS of the oligosaccharides derived the total non-acid glycosphingolipid fraction from porcine lung by digestion with *Rhodococcus* endoglycoceramidase II. B. Base peak chromatogram from LC-ESI/MS of the oligosaccharides derived the total non-acid glycosphingolipid fraction from porcine erythrocytes by digestion with *Rhodococcus* endoglycoceramidase II. The identification of individual glycosphingolipid-derived oligosaccharides was based on their determined molecular masses and subsequent MS^2 sequencing. The oligosaccharides identified in the chromatograms are: Gb3, Galα1–4Galβ1–4Glc; H5-2, Fucα2–3Galβ1–4GlcNAcβ1–3Galβ1–4Glc; B5, Galα1–3Galβ1–4GlcNAcβ1–3Galβ1–4Glc;

Gb4, GalNAcβ1–3Galα1–4Galβ1–4Glc; A6-2, GalNAcα1–3(Fucα2–3)Galβ1–4GlcNAcβ1–3Galβ1–4Glc. **B. SadP binding tri- and tetraglycosylceramides isolated from porcine lung.** Thin-layer chromatogram after detection with anisaldehyde (A), and autoradiograms obtained by binding of SadP (B), followed by autoradiography for 12 h, as described under "Methods". The solvent system used was chloroform/methanol/water (60:35:8, by volume). The lanes were: Lane 1, fraction PL-1 isolated from pig lung, 1 μg; Lane 2, fraction PL-2 isolated from pig lung, 1 μg; Lane 3, fraction PL-3 isolated from pig lung, 1 μg; Lane 4, fraction PL-4 isolated from pig lung, 1 μg; Lane 5, reference globotetraosylceramide (GalNAcβ1–3Galα1–4Galβ1–4Glcβ1Cer), 2 μg; Lane 6, reference globotriaosylceramide (Galα1–4Galβ1–4Glcβ1Cer), 2 μg. **C. TLC overlay assay with purified glycolipids**, **SadP-D282 type P_N** 1. Gb2, galabiaosylceramide 2 μg, 2. iGb3, isoglotriosylceramide 4 μg, 3 Gb3, globotriosylceramide 4 μg , 4. Gb4, globotetraosylceramide 4 μg, 5. Gb5, Forssman 4 μg, 6. P1 pentaosylceramide 4 μg. **D. SadP-6407 type P_O** 1. Lactosylceramide 4 μg, 2. Galabiaosylceramide 4 μg, 3. Globotriaosylceramide 4 μg, 4. Globotetraosylceramide 4 μg, 5. P1, pentaosylceramide 4 μg, 6. Forssman pentaosylceramide 4 μg, 7. Non-acid glycosphingolipids of porcine small intestine (blood group O) 40 μg.

Fig 3. SadP binding to EA.hy926 cell line. A. Binding of S. suis D282 wild type serotype 2 strain and the SadP insertion mutation to EA.hy926 cells grown on coverslips. The binding of the wild type bacteria was inhibited with 10 μg/ml of pigeon ovomucoid. Flow cytometry analysis of SadP(31-328) type P_N binding to EA.hy926 cells. **B.** Buffer control. **C.** SadP adhesin (0.4 μg/ml) and **D.** SadP adhesin in the presence of 10 μg/ml of pigeon ovomucoid.

Fig 4. Oligosaccharide specificity of SadP from systemic (type P_N) and respiratory (type P_O) *S. suis* strains analyzed with glycans representing the terminal saccharide structure of Gb3 and Gb4. A. and B. ITC of SadP type P_N and type P_O with Galα1–4Galβ1– and GalNAcβ1–3Galα1–4Galβ1– TMSEt derivatives **C.** AlphaScreen inhibition assay with Galα1–4Galβ1– and 3'Phenylurea-Galα1–4Galβ1–methoxyphenyl (-PMP = 4-methoxyphenyl). **D**. AlphaScreen inhibition assay of Galα1–4Galβ1– (compound

C10) and 3'Phenylurea-Galα1–4Galβ1– methoxyphenyl (compound C53) with recombinant N-terminal domains cloned from 4 different type P_O *S. suis* strains **E**. Structures of the ligands in this study.

Fig 5. A. Single amino acid site-specific mutation N285D of SadP from systemic strains changes its Gb4 binding specificity to type P_O Gb3 binding specificity of respiratory strains. A. Inhibition of WT SadP(125-329) and its site-specific mutant SadP(125-329)N285D with the dilutions series (1.25 to 320 μM, duplicate determinations) of TMSEt (2-trimethylsilylethyl) glycosides of Galα1–4Gal and GalNAcβ1–3Galα1–4Gal representing the Gb3 and Gb4 oligosaccharides. **B.** Inhibition assay with 5 μM of Galα1–4Gal and GalNAcβ1–3Galα1–4Gal TMSEt glycosides. **C.** ITC measurements of WT SadP and N285D mutant with the TMSEt glycosides of Galα1–4Gal and GalNAcβ1–3Galα1–4Gal representing the Gb3 and Gb4 oligosaccharides.

Fig 6. SadP and $SadP_{N285D}$ binding to liposomes. POPC/glycolipid liposomes (4, 0.4 and 0.04 nmol/dot) and POPC/cholesterol/globosylceramide liposomes (4, 0.4 and 0.04 nmol/dot) were applied onto PVDF membrane. WT, His-tagged SadP(125-329) type P_N; N285D, site-specific mutant of SadP(125-329); Replicate membranes containing dotted liposomes with or without cholesterol (see Methods) were probed with **SadP and $SadP_{N285D}$**. The bound proteins were detected with anti-His and HRP-labelled antibodies as described in the methods and membrane was imaged with FujiLAS-4000. The globo series glycolipids used were: Gb4, d18:1-24:0 + d18:1 – 16:0; Gb3/1, Gb3 d18:1-24:0; Gb3/2, Gb3 d18:1-16:0; Gb3/3, Gb3 d18:1-h16:0.

Fig 7. A. Arrangement of the five site-specifically mutated SadP(125-329)N285D molecules in the crystallographic asymmetric unit. Each molecule is shown as ribbon and colored differently. **B.** Ribbon diagram of SadP(125-329)N285D structure. α-Helices are shown in yellow color and β-strands in cyan. D285 is depicted as sticks. **C.** Structural superposition of Galα1–4Gal -bound Fhc (PDB 5BOA) structure (identical to SadP type P_N (pink) onto $SadP(125\text{-}329)_{N285D}$ (cyan). Residues involved in binding interactions are shown

in stick representation. **D.** STD-NMR of binding of wild type SadP(125-329) type P_N and its site-specific mutant N285D. Peaks in the STD spectra indicate hydrogens (C-H) that are in close proximity to the protein.

Fig 8. Molecular dynamics of SadP type P_N binding to Gb4 saccharide and glycomimetic phenylurea-galabiose inhibitor. Representative MD snapshots (at 90 ns) of SadP. WT in complex with **A**. Galα1–4Gal, **B**. GalNAcβ1–3Galα1–4Galβ, and **C.** C3´-phenylurea-Galα1–4Galβ. Representative MD snapshots of SadP N285D in complex with **D.** Galα1–4Gal, **E.** GalNAcβ1–3Galα1–4Galβ, and **F.** C3´-phenylurea-Galα1–4Galβ.

Fig 9. Summary of the results. A. SadP type P_N (cyan) and type P_O (green) are putative duplicates of the downstream SadP homolog (grey). **B.** Conservative change of type P_N SadP asparagine-285 to aspartic acid of SadP type P_O. **C.** This study has shown the mechanism how N285 contributes to the binding of terminal GalNAcβ1- saccharide of Gb4 by a specific interaction with GalNAc hexose ring oxygen (orange dashed line). The 3D-structure of SadP type P_O from type 4 *S. suis* 6407 was obtained by homology modelling (Swiss Prot) and superimposed structures of type P_N (cyan) in complex with GalNAcβ1–Galα1–4Gal and type P_O (green) were created with Pymol. The structures suggest that the abolishment of Gb4 binding is based on the same mechanism as shown with N285D mutant. **D.** The results of the binding mechanisms of SadP type P_N with Gb4 and the distribution of SadP subtypes in *S. suis* clinical and non-clinical strains suggest that SadP Gb4 binding is associated with strains causing systemic disease. Therefore, the molecular mechanism of SadP type P_N binding to Gb4 could be targeted to prevent *S. suis* systemic diseases.

Supporting information

S1 Fig. LC-ESI/MS of the native fraction PL-1 from pig lung. (A) Base peak chromatogram from LC-ESI/MS of fraction PL-2 from pig lung. (B) MS^2 of the ion at *m/z* 1132 (retention time 14.1 min). The interpretation formula shows the deduced glycosphingolipid structure.

S2 Fig. LC-ESI/MS of the native fraction PL-2 from pig lung. (A) Base peak chromatogram from LC-ESI/MS of fraction PL-2 from pig lung. (B) Mass chromatogram of *m/z* 1022. (C) Mass chromatogram of *m/z* 1132. (D) MS^2 of the ion at *m/z* 1022 (retention time 13.1 min). (E) MS^2 of the ion at *m/z* 1132 (retention time 12.5 min). (F) Interpretation formulas showing the deduced glycosphingolipid structures.

S3 Fig. LC-ESI/MS of the oligosaccharides obtained by digestion of fraction PL-1, PL-2, reference globotriaosylceramide, and reference isoglobotriaosylceramide with *Rhodococcus* endoglycoceramidase II. A. Base peak chromatogram from LC-ESI/MS of the oligosaccharides derived from fraction PL-1. B. Base peak chromatogram from LC-ESI/MS of the oligosaccharides derived from fraction PL-2. C. Base peak chromatogram from LC-ESI/MS of the oligosaccharides derived from reference globotriaosylceramide (Galα1–4Galβ1–4Glcβ1–O–Cer). D. Base peak chromatogram from LC-ESI/MS of the oligosaccharides derived from reference isoglobotriaosylceramide (Galα1–3Galβ1–4Glcβ1–O–Cer). E. MS^2 of the ion at *m/z* 503 (retention time 18.4 min) in (A). F. MS^2 of the ion at *m/z* 503 (retention time 17.7 min) in (B). G. MS^2 of the ion at *m/z* 503 (retention time 17.4 min) in (C). H. MS^2 of the ion at *m/z* 503 (retention time 20.2 min) in (D). The interpretation formula shows the deduced oligosaccharide structure. The identification of oligosaccharides was based on their retention times, determined molecular masses and subsequent MS^2 sequencing.

S4 Fig. LC-ESI/MS of the oligosaccharides obtained by digestion of fraction PL-4, and reference globotetraosylceramide with *Rhodococcus* endoglycoceramidase II. A. Base peak chromatogram from LC-ESI/MS of the oligosaccharides derived from fraction PL-4. B. MS^2 of the ion at *m/z* 706 (retention time 18.4 min) in (A). C. MS^2 of the ion at *m/z* 706 (retention time 18.6 min) from LC-ESI/MS of the oligosaccharides

derived from reference globotetraosylceramide (GalNAcβ1–3Galα1–4Galβ1–4Glcβ1–O–Cer). D. MS^2 of the ion at *m/z* 998 (retention time 19.4 min) in (A). E. MS^2 of the ion at *m/z* 998 (retention time 21.4 min) in (A). The interpretation formula shows the deduced oligosaccharide structure. The identification of oligosaccharides was based on their retention times, determined molecular masses and subsequent MS^2 sequencing.

S5 Fig. SadP types P_N and P_O glycolipid binding specificity analysed with TLC overlay analysis and microwell binding assay: A. Decreasing glycolipid dilutions from 2 to 0.2 µg per lane probed with SadP type P_N full length and it's N-terminal domain SadP(31-328). **B.** Microwell binding assay with radiolabelled SadP type P_N to 250 ng of glycolipids, Gb2 galabiosylceramide, Gb2-S Galα1–4Galβ1–O-*bis*-(SO_2-$C_{16}H_{33}$)$_2$, Gb3 non-OH globotriaosylceramide with non-hydroxy ceramide, Gb3 OH globotriaosylceramide with hydroxy ceramide, iGb3 isoglobotriaosylceramide, Gb4, globotetraosylceramide, P1 pentaosylceramide. Leb Lewis b hexaosylceramide.

S6 Fig. SDS-PAGE of the type P_N WT SadP(125-329) and the site-specific mutants N285D and E292Q, deletion Δ244-246 and N285D&Δ244-246 mutants were constructed into the type P_N SadP(125-328) cloned into the plasmid pET28a. In addition, the 28 amino acid long region H216-D246 of the type P_N was replaced by the corresponding region of type P_O.

S7 Fig. A. Binding of SadP wild type and site-specific mutants to Galα1–4Gal analysed with AlphaScreen**. B - F.** Inhibition assay for the binding of site-specific mutants of PSAD1-5 (PSAD-1 Δ244-246, PSAD-2 N285D, PSAD-3 E292Q, PSAD-4 N285D&Δ244-246 and PSAD-5 H216-D246delinsDELFNRFPNKVDSTNNGDGAPFRFFNKE (replacement of aa 216-242 into corresponding sequence of type P_O of strain 6107).

S8 Fig. Structure analysis of TMSEt (2-trimethylsilylethyl) glycosides

S9 movie. MD simulation of type P_N WT SadP(125-329) and Galα1–4Gal

S10 movie. MD simulation of N285D SadP(125-329) and Galα1–4Gal

S11 movie. MD simulation of of type P_N WT SadP(125-329) and GalNAcβ1–3Galα1–4Gal

S12 movie. MD simulation of of type P_N WT SadP(125-329) and 3'-phenylurea- Galα1–4Gal

S13 movie. MD simulation of N285D SadP(125-329) and GalNAcβ1–3Galα1–4Gal

S14 movie. MD simulation of N285D SadP(125-329) and 3'-phenylurea- Galα1–4Gal